OKLAHOMA TRANSPORTATION CENTER

ECONOMIC ENHANCEMENT THROUGH INFRASTRUCTURE STEWARDSHIP

REPAIR AND RETROFIT OF CONCRETE GIRDERS USING HYBRID FRP SHEETS

THOMAS H.-K. KANG, WOOSUK KIM, AMY HUFNAGEL,
MOUSTAPHA ARY IBRAHIM, YU HUANG, DONG-UK CHOI,
CHIN YONG LEE, LISA HOLLIDAY

OTCREOS10.1-21-F

Oklahoma Transportation Center
2601 Liberty Parkway, Suite 110
Midwest City, Oklahoma 73110

Phone: 405.732.6580
Fax: 405.732.6586
www.oktc.org

TECHNICAL REPORT DOCUMENTATION PAGE

1. REPORT NO.	2. GOVERNMENT ACCESSION NO.	3. RECIPIENTS CATALOG NO.
OTCREOS10.1-21-F		

4. TITLE AND SUBTITLE	5. REPORT DATE
Repair and Retrofit of Concrete Bridge Girders Using Hybrid FRP Sheets	February 2012
	6. PERFORMING ORGANIZATION CODE
7. AUTHOR(S)	8. PERFORMING ORGANIZATION REPORT
Thomas H.-K. Kang, Woosuk Kim, Amy Hufnagel, Moustapha Ary Ibrahim, Yu Huang, Dong-Uk Choi, Chin Yong Lee, Lisa Holliday	
9. PERFORMING ORGANIZATION NAME AND ADDRESS	10. WORK UNIT NO.
The University of Oklahoma School of Civil Engineering & Environmental Science 202 W. Boyd St. Rm 334, Norman, OK 73019	
	11. CONTRACT OR GRANT NO. DTRT06-G-0016
12. SPONSORING AGENCY NAME AND ADDRESS	13. TYPE OF REPORT AND PERIOD COVERED
Oklahoma Transportation Center (Fiscal) 201 ATRC Stillwater, OK 74078 (Technical) 2601 Liberty Parkway, Suite 110, Midwest City, OK 73110	Final: Jan. 2010 - Feb. 2012
	14. SPONSORING AGENCY CODE

15. SUPPLEMENTARY NOTES
University Transportation Center

16. ABSTRACT

The use of carbon fibers (CF) and glass fibers (GF) were combined to strengthen potentially non-ductile flexural members. Based on tension tests of fiber-reinforced polymer (FRP) rovings and sheets, as well as theoretical research on hybrid FRP, a volume ratio of (GF/CF) was determined to be about (8.8/1) to produce synergistic hybrid effects and pseudo-ductility. The (8.8/1) ratio was used to fabricate hybrid carbon-glass FRP sheets, and this optimal combination was verified through four-point loading tests of plain and reinforced concrete beams strengthened with single or multiple plies of FRP sheets. The increased flexural strengths were evaluated using available design procedures in conjunction with a proposed force-strain relationship for hybrid carbon-glass FRP sheets.

Additionally, data of tensile tests of 94 hybrid carbon-glass FRP sheets and 47 carbon and glass fiber rovings or sheets were thoroughly re-examined in terms of tensile behavior. Based on thorough comparisons between the rule of mixtures for fibrous composites and test data, positive hybrid effects were clearly identified for almost all (GF/CF) ratios. In contrast to the rule of mixtures, the hybrid sheets with relatively low (GF/CF) ratios also produced pseudo-ductility. From the calibrated results obtained from experiments, a novel analytical model for the stress-strain relationship of hybrid FRP sheets was proposed. The effect of various epoxy resins, impregnating degree and specimen grips on the tensile behavior was minimal.

17. KEY WORDS	18. DISTRIBUTION STATEMENT
Fiber-reinforced polymers, carbon fibers, glass fibers, pseudo-ductility, hybrid effects, rule of mixtures, reinforced concrete beams, repair, retrofit	No restrictions. This publication is available at www.oktc.org and at the NTIS: National Technical Information Service Springfield, Virginia 22161 http://www.ntis.gov

19. SECURITY CLASSIF. (OF THIS REPORT)	20. SECURITY CLASSIF. (OF THIS PAGE)	21. NO. OF PAGES	22. PRICE
Unclassified	Unclassified	82 + covers	

SI (METRIC) CONVERSION FACTORS

Approximate Conversions to SI Units

Symbol	When you know	Multiply by	To Find	Symbol
	LENGTH			
in	inches	25.40	millimeters	mm
ft	feet	0.3048	meters	m
yd	yards	0.9144	meters	m
mi	miles	1.609	kilometers	km
	AREA			
in^2	square inches	645.2	square millimeters	mm
ft^2	square feet	0.0929	square meters	m^2
yd^2	square yards	0.8361	square meters	m^2
ac	acres	0.4047	hectares	ha
mi^2	square miles	2.590	square kilometers	km^2
	VOLUME			
fl oz	fluid ounces	29.57	milliliters	mL
gal	gallons	3.785	liters	L
ft^3	cubic feet	0.0283	cubic meters	m^3
yd^3	cubic yards	0.7645	cubic meters	m^3
	MASS			
oz	ounces	28.35	grams	g
lb	pounds	0.4536	kilograms	kg
T	short tons (2000 lb)	0.907	megagrams	Mg
	TEMPERATURE (exact)			
°F	degrees Fahrenheit	(°F-32)/1.8	degrees Celsius	°C
	FORCE and PRESSURE or STRESS			
lbf	poundforce	4.448	Newtons	N
lbf/in^2	poundforce per square inch	6.895	kilopascals	kPa

Approximate Conversions from SI Units

Symbol	When you know	Multiply by	To Find	Symbol
	LENGTH			
mm	millimeters	0.0394	inches	in
m	meters	3.281	feet	ft
m	meters	1.094	yards	yd
km	kilometers	0.6214	miles	mi
	AREA			
mm^2	square millimeters	0.00155	square inches	in^2
m^2	square meters	10.764	square feet	ft^2
m^2	square meters	1.196	square yards	yd^2
ha	hectares	2.471	acres	ac
km^2	square kilometers	0.3861	square miles	mi^2
	VOLUME			
mL	milliliters	0.0338	fluid ounces	fl oz
L	liters	0.2642	gallons	gal
m^3	cubic meters	35.315	cubic feet	ft^3
m^3	cubic meters	1.308	cubic yards	yd^3
	MASS			
g	grams	0.0353	ounces	oz
kg	kilograms	2.205	pounds	lb
Mg	megagrams	1.1023	short tons (2000 lb)	T
	TEMPERATURE (exact)			
°C	degrees Celsius	9/5+32	degrees Fahrenheit	°F
	FORCE and PRESSURE or STRESS			
N	Newtons	0.2248	poundforce	lbf
kPa	kilopascals	0.1450	poundforce per square inch	lbf/in^2

ACKNOWLEDGMENTS

The authors would like to express their appreciation to the following REU students and collaborators, who assisted the execution of the laboratory work.

Deanna Quickle, Undergraduate student from Stony Brook University;

Caroline Weston, Undergraduate student from Southwestern University;

Sang-Su Ha, Ph.D., Full-time Lecturer at Kangnam University, Korea;

Chris Ramseyer, Ph.D., P.E., Assistant Professor at the University of Oklahoma.

Also, it is noted that the first author completely analyzed and re-analyzed the raw data provided by the seventh author, Dr. Chin Yong Lee, who was the Principal Investigator of the test program presented in Sections 8.2 and 10.2 and Chapter 11, and that the first author was the writer of this final report.

REPAIR AND RETROFIT OF CONCRETE BRIDGE GIRDERS USING HYBRID FRP SHEETS

Final Report

February, 2012

Thomas H.-K. Kang, Ph.D., P.E.
Assistant Professor, Department of Architecture & Architectural Engineering,
Seoul National University, Korea
and
Adjunct Professor, School of Civil Engineering & Environmental Science,
The University of Oklahoma

Woosuk Kim, Ph.D., Amy Hufnagel, M.S., Moustapha Ary Ibrahim, M.S., Yu Huang, Ph.D.
Research Assistants, School of Civil Engineering & Environmental Science,
The University of Oklahoma

Dong-Uk Choi, Ph.D.
Professor, Department of Architectural Engineering,
Hankyong National University, Korea

Chin Yong Lee, Ph.D.
President, Carecon, Korea
and
Adjunct Faculty, Department of Civil Engineering, Dongguk University, Korea

Lisa Holliday, Ph.D., P.E.
Assistant Professor, Division of Construction Science
The University of Oklahoma

School of Civil Engineering and Environmental Science
The University of Oklahoma
202 W. Boyd St., Room 334
Norman, OK 73019

TABLE OF CONTENTS

LIST OF FIGURES

LIST OF TABLES

EXECUTIVE SUMMARY

This study aims to optimize hybrid carbon-glass fiber-reinforced polymer sheets to repair and retrofit existing concrete bridges. Over the last half-century, highway concrete infrastructures have aged, exposing both apparent and invisible damages associated with concrete deterioration, reinforcing and prestressing steel corrosion, and fatigue loading-induced large deformations. The use of fiber-reinforced polymer (FRP) sheets has been common to repair and improve such infrastructures.

In concrete structures strengthened using FRP materials, however, the brittleness is inherent due to the linear stress-strain characteristics of fibers up to ruptures. To overcome this disadvantage, applications of hybrid carbon-glass FRP sheets are proposed. The hybrid FRP sheet provides a superior alternative to costly repair, since they cost only about 40% as much as carbon FRP sheets of comparable strength, as well as exhibit desired pseudo-ductility. Such economic and technological advancements support the OTC strategic vision that promotes innovation and efficiency through synergetic uses of novel materials.

Based on tension tests of fiber-reinforced polymer (FRP) rovings and sheets, as well as theoretical research on hybrid FRP, a volume ratio of (GF/CF) was determined to be about (8.8/1) to produce synergistic hybrid effects and pseudo-ductility. The (8.8/1) ratio was used to fabricate hybrid carbon-glass FRP sheets, and this optimal combination was verified through four-point loading tests of plain and reinforced concrete beams strengthened with single or multiple plies of FRP sheets. The increased flexural strengths were evaluated using available design procedures in conjunction with a proposed force-strain relationship for hybrid carbon-glass FRP sheets.

Additionally, data of tensile tests of 94 hybrid carbon-glass FRP sheets and 47 carbon and glass fiber rovings or sheets were thoroughly re-examined in terms of tensile behavior. Based on thorough comparisons between the rule of mixtures for fibrous composites and test data, positive hybrid effects were clearly identified for almost all (GF/CF) ratios. In contrast to the rule of mixtures, the hybrid sheets with relatively low

(GF/CF) ratios also produced pseudo-ductility. Based on the calibrated results obtained from experiments, a novel analytical model for the stress-strain relationship of hybrid FRP sheets was proposed. The effect of various epoxy resins, impregnating degree and specimen grips on the tensile behavior was minimal.

In large part, international collaboration was pursued vigorously to make maximum use of U.S. investments. One of the goals of the project was eventually to address transportation agencies' needs and provide practical guidelines for design and field engineers. Furthermore, a wide array of education and diversity programs were offered as part of the project.

PART I

1.1 INTRODUCTION TO PART I

Before the 1990's, steel plates had been typically used to strengthen concrete structures; however, because steel plates increase dead loads and are vulnerable to corrosion, fiber-reinforced polymer (FRP) sheets or wraps have replaced steel in repair applications. Despite the relatively expensive cost, carbons fibers (CF) and carbon FRP sheets have been primarily used for repair and retrofit. This is attributed to the fact that CF has high durability, high elastic modulus (E_{CF}), and high ultimate strength (f_{u_CF}) (see Figure 1). Glass fibers (GF) are also popular, as they only cost about 5 to 10% as much as CF; however, GF has much less ultimate stress (f_{u_GF} between f_{u_CF} and f_y) and very low elastic modulus (E_{GF}) – only 1/3 to 1/5 of that of steel (E_s), where f_y is the specified yield stress of steel (Figure 1).

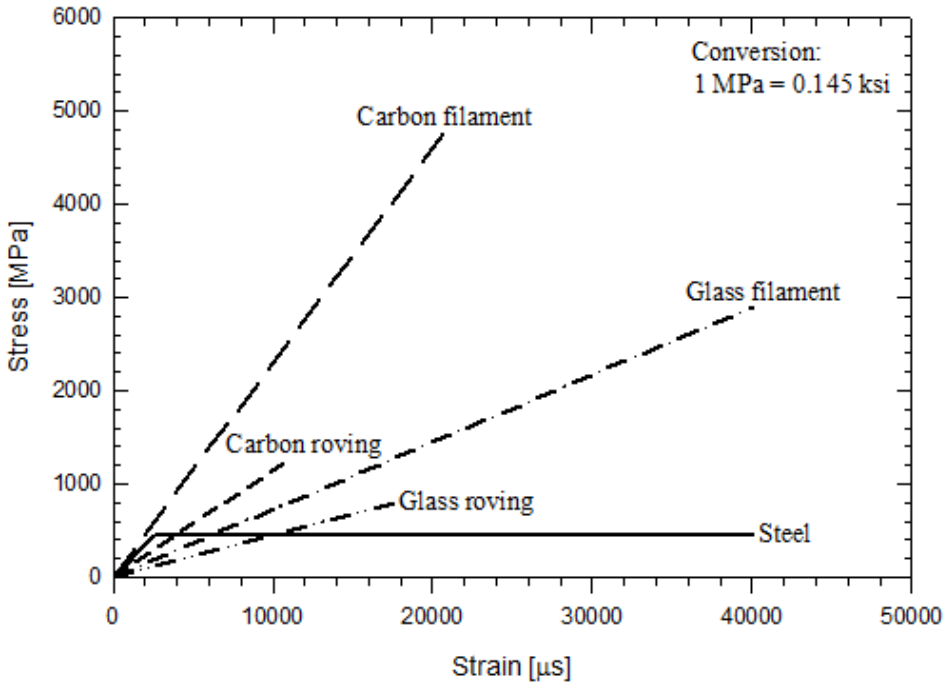

Figure 1 Stress-Strain Relations for Steel, Fiber Filaments, Rovings and Hybrid FRP Sheets (Scaled Based on the Measured and Provided Material Properties)

In concrete structures strengthened using FRP materials, however, the brittleness is inherent due to the linear stress-strain characteristics of all these fibers up to ruptures (i.e., little nonlinearity; see Figure 1). In order to avoid such a brittle failure, previous research was conducted on hybrid FRP materials combining multiple fiber types [1], [2]. Applications of uni-axial hybrid FRP bars or sheets on concrete have been studied by several researchers [3], [4], [5]. Grace et al. [5] used three fibrous materials of ultra-high-modulus CF, high-modulus CF, and high-ductility E-glass fibers to provide "pseudo-ductility" similar to the ductile response of nonlinear steel materials, while Wu et al. [4] tested concrete cylinders wrapped by different combinations of fibrous materials such as carbon, glass, or aramid fibers to observe a recovery of ductility. Pseudo-ductility can be defined by the writers as follows: (1) after the first fiber failure (first drop in load), the load carrying capacity is maintained or improved as the remaining fibers stretch with increases in deflection; and (2) the strain at ultimate failure of hybridized fibers is not less than the ultimate strain of any fiber.

In the current study, hybrid fibrous sheets using two different types of fibers (CF and GF) are developed in such a way that the glass-to-carbon volume (GF/CF) ratio would be optimal for strengthening a lightly-reinforced concrete beam. When the hybrid FRP sheet is subjected to tension, the CF with high elastic modulus and low ultimate strain ruptures first. The GF, with lower elastic modulus and higher ultimate strain, then takes over and resists the load. The clear sound warning is produced when the first fibers (CF) rupture, indicating the distress and possible impending failure of the structure. In this study, uni-axial hybrid fibrous sheet is first developed and fabricated using carbon and glass fibers (see Figure 2), followed by experimental verification of performance of concrete beams strengthened with the hybrid FRP sheet.

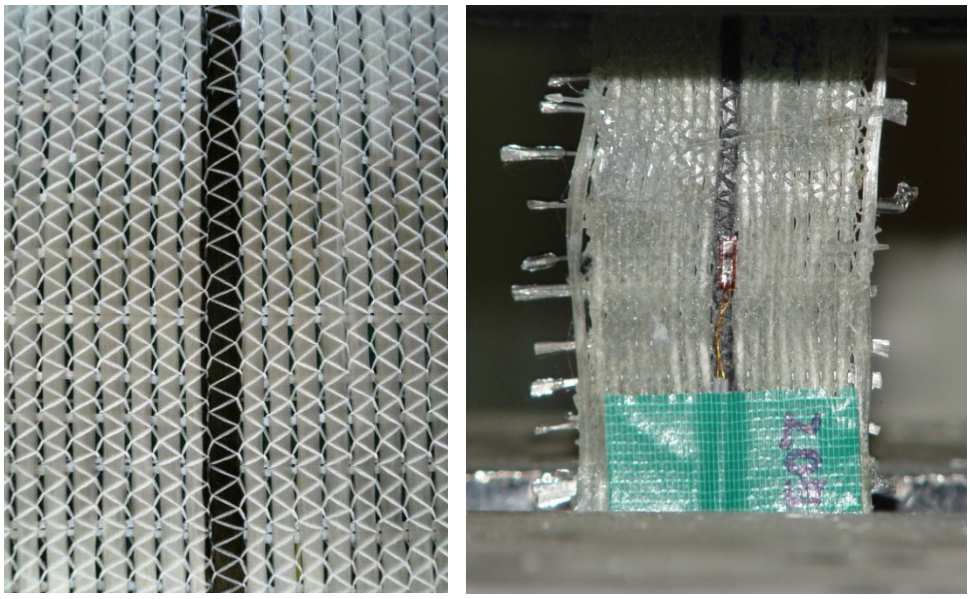

Figure 2 Fabricated Carbon-Glass Hybrid FRP Sheet and Its Tensile Test (Black: A Carbon Fiber Roving; White: Glass Fiber Rovings)

The current study consists of basic material tests, concrete beam experiments, force-strain behavior modeling and section analyses. In the first part, material properties were examined using Scanning Electron Microscopy and coupon tests of fiber rovings, sheets, and epoxy adhesives. In the second part, the experimental program consists of 1) flexural testing of small-scale plain concrete beams strengthened using fiber rovings; 2) flexural testing of large-scale reinforced concrete beams strengthened using conventional and hybrid FRP sheets; and 3) bond testing of hybrid carbon-glass FRP sheets attached to concrete blocks. Furthermore, moment capacities of the beams with the hybrid sheets are evaluated using ACI 440.2R-08 report [6] and ISIS Canada Design Manual No. 4 [7], in connection with a proposed force-strain relationship of hybrid carbon-glass FRP sheets.

1.2 RESEARCH SIGNIFICANCE

The hybrid carbon-glass FRP sheet provides a superior alternative to costly repair, since they cost only about 40% as much as carbon FRP sheets of comparable strength, as well as exhibit desired pseudo-ductility. A volume ratio between carbon and glass fibers that maximizes the pseudo-ductility was found through theoretical and experimental techniques, including structural tests of 22 concrete beams and material tests of fiber rovings, sheets and epoxy adhesives. Finally, a force-strain relationship for hybrid FRP sheets was proposed, based on which analytical studies were conducted to obtain a balanced ratio between the hybrid sheet and tensile reinforcing steel amounts for each given glass-to-carbon ratio.

2. MATERIALS AND MATERIAL TESTS

In this chapter, all materials are described in detail, including carbon and glass fibers (filament and roving), hybrid carbon-glass FRP sheets, and epoxy adhesives, as well as concrete and reinforcing steel.

2.1 CONCRETE AND REINFORCING STEEL

All results for concrete and reinforcing steel bars tested are summarized in Table 1, and representative stress-strain relationships of concrete and steel are depicted in Figure 3. In Table 1, results of three concrete cylinders and two coupons of steel bars were each averaged. All reinforcing bars used for flexural tests have a diameter of 0.39 in. (10 mm) and specified yield stress of 58 ksi (400 MPa). For bond tests, the same type of bars but with a different diameter of 0.75 in. (19 mm) was used.

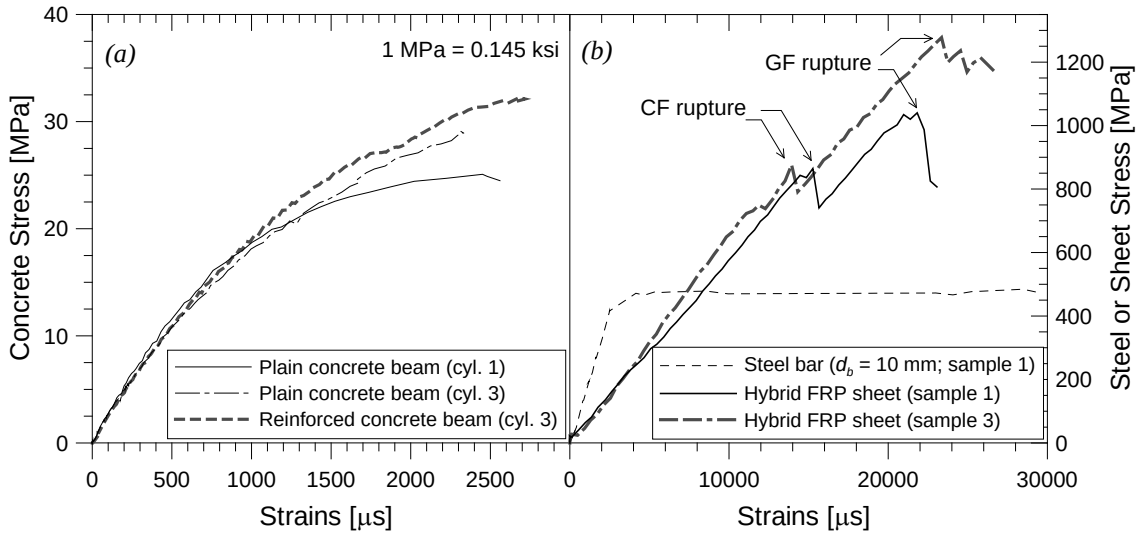

Figure 3 Measured Stress-Strain Relations for Concrete, Steel and Hybrid FRP Sheets

Table 1 Measured and Provided Material Properties

	Elastic Modulus (GPa)	Stress at Failure (MPa)	Corresponding Strain
Concrete	NA	26[a] / 29.5[b] / 22.3[c]	NA
Steel	164.5	446.5[d] / 559[e]	0.0026[d] / NA[e]
CF filament[†]	230	4,900	0.0213
CF roving[††]	114 (= E_{CF})	1,280 (= f_{u_CF})	0.0112
CF roving[‡]	NA	1,555	NA
GF filament[†]	72.5	2,900	0.0401
GF roving[††]	45 (= E_{GF})	792 (= f_{u_GF})	0.0176
GF roving[‡]	NA	764	NA
HF sheet	62.1	842[f] / 1,094[g]	0.014[f] / 0.022[g]

Note: CF = Carbon Fiber; GF = Glass Fiber;
HF = Hybrid FRP; NA = Not Available
[†]: Provided by the manufacturer
[††]: Average of 10 non-impregnated (bare) roving tests
[‡]: Average of 9 (CF) or 10 (GF) impregnated roving tests (per ASTM D3039-08)
[a]: peak stress for plain concrete beam tests; [b]: peak stress for RC beam tests;
[c]: peak stress for bond tests; [d]: at yielding; [e]: at ultimate;
[f]: at CF rupture; [g]: at GF rupture (= f_{u_HF})
Conversion: 1 GPa = 145 ksi; 1 MPa = 0.145 ksi

2.2 EPOXY ADHESIVES

Mechanical properties of epoxy adhesives used to bond FRP sheets to concrete were examined. Since the adhesive flexural strength is often a governing factor (ACI 503.5R-92 [8]) and the direct tensile test gives a tensile strain somewhat smaller than the actual strain of the adhesive bonded to concrete (ASTM D638 [9]), in this study, epoxy solid blocks with dimensions of 1 x 1 x 9.5 in. (25 x 25 x 240 mm) were tested in flexure under three-point loading. The resulting average values of ultimate stress (f_u) and strain (ε_u), and modulus of elasticity (E) at rupture for three specimens are 6.2 ksi (42.8 MPa), 0.0197 and 317.6 ksi (2.19 GPa), respectively, which are similar to the typical values

reported by ACI 503R-93 [10]. The ε_u of the product was relatively low. It would be useful to have about 0.04 to ensure that fiber ruptures prior to epoxy failure [5].

2.3 FIBROUS MATERIALS

Figure 4 shows microscopic cross-sectional views of carbon and glass fiber rovings taken by Scanning Electron Microscopy. The cross-sectional views indicate that the diameters of CF and GF filaments are approximately 0.28×10^{-3} and 0.8×10^{-3} in. (7.23×10^{-3} and 20.5×10^{-3} mm), respectively. Using each fiber's Specific Gravity ($\rho_{CF} = 1.8$; $\rho_{GF} = 2.54$) and measured weight per unit length, the cross-sectional area was determined to be 6.9×10^{-4} and 1.34×10^{-3} in^2 (0.444 and 0.866 mm^2) for the tested CF and GF rovings, respectively (Table 1). The weight of the fiber roving was measured using a digital scale with an accuracy of $+/-2.2 \times 10^{-5}$ lbs (or 1/100 g). It is not recommended to calculate the cross-sectional area by manually measuring the thickness and width of FRP sheets. Rather, in the field, the area (in units of cm^2) should be taken as the fiber's Specific Gravity (= [density of fibers / density of water] = [density of fibers / (1 g/cm^3 = 62.4 lb/ft^3)]), divided by the measured total weight (in units of g) and the length (in units of cm) of the roving or sheet. The thickness should then be determined as the area divided by the width.

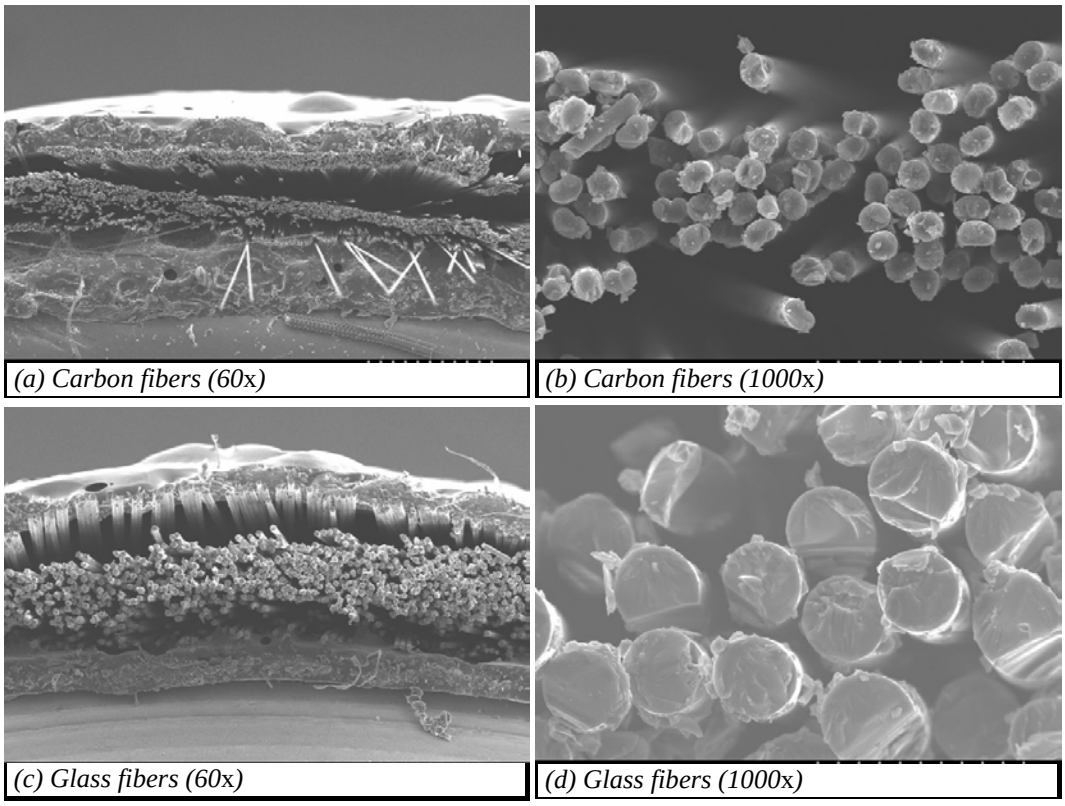

(a) Carbon fibers (60x) | *(b) Carbon fibers (1000x)*

(c) Glass fibers (60x) | *(d) Glass fibers (1000x)*

Figure 4 Microscopic Cross-Sectional Views of Carbon and Glass Fiber Rovings Taken by Scanning Electron Microscopy

Average results from tensile tests of 10 coupons of bare CF and GF rovings, respectively, are presented in Table 1 and Figure 1. Additionally, 9 and 10 coupons of the impregnated CF and GF rovings, respectively, with two different grip types (epoxy block and epoxy block with transverse rovings embedded) were tested, as per ASTM D3039-08 [11] (Table 1). Although ACI 440.2R-08 [6], Section 4.3.1 recommends using mean minus three times standard deviations for f_u and ε_u from at least 20 roving tests, the mean stress and strain (f_u and ε_u) from the non-impregnated (bare) coupon tests were used for the remaining of the paper (though both results are similar). This is because epoxy resins are typically applied on only one side of the FRP sheet (Table 1). During the tensile tests, force and strain values were read directly from the monitor of a

Universal Test Machine with a full load capacity of 112.4 lbs (500 N). The roving results for ultimate stress (f_u), ultimate strain (ε_u) and elastic modulus (E) in tension are substantially lower than the filament properties provided by the manufacturer (Figure 1). This appears due to unequal tension in filaments within rovings and their sequential failures. Such phenomena are closer to actual behavior of FRP sheets externally bonded to the concrete surface, as observed from beam tests described later in this report.

2.4 HYBRID CARBON-GLASS FRP SHEETS

Chou and Kelly [12], and Manders and Bader [2] proposed a theoretical tensile stress model for hybrid carbon-glass FRP as shown in Figure 5(a). Points A and D denote the ultimate tensile stresses when GF and CF are used alone (i.e., GF = 100%; CF = 100%), respectively. Also, the lines A-E and B-D represent the mean stresses in hybrid FRP when the strain reaches the GF and CF ultimate strains (ε_{u_GF} and ε_{u_CF}), respectively. The CF with lower ε_{u_CF} than ε_{u_GF} (or higher $E_{\_CF}$ than $E_{\_GF}$) always fails prior to GF. To the right of Point C, after the first failure of CF, the hybrid FRP has a very low residual mean stress that is only provided by GF (i.e., brittle failure). To the left of Point C, even after the first failure of CF, the hybrid FRP with a relatively large amount of GF can sustain more loads without a drop in strength until the GF rupture. As such, the pseudo-ductility can be achieved with this combination.

Based on the roving tests, Points A and D are determined to be 114.8 and 185.6 ksi (792 and 1280 MPa), respectively (see Table 1), for this study. The mean stress at Point B is calculated as ε_{u_CF} times E_{GF} (= 0.0112 x 6,525 ksi = 73 ksi; 0.0112 x 45,000 MPa = 504 MPa). Using the theoretical model by Manders and Bader (1981) and the test data, the x- and y-axes' values at Point C are determined to be (4.4/1) and 94.25 ksi (650 MPa), respectively. This is obtained from a cross point of two straight lines drawn in Figure 5(a). The ratio of (4.4/1) is equivalent to the carbon volume fraction of 18.4%.

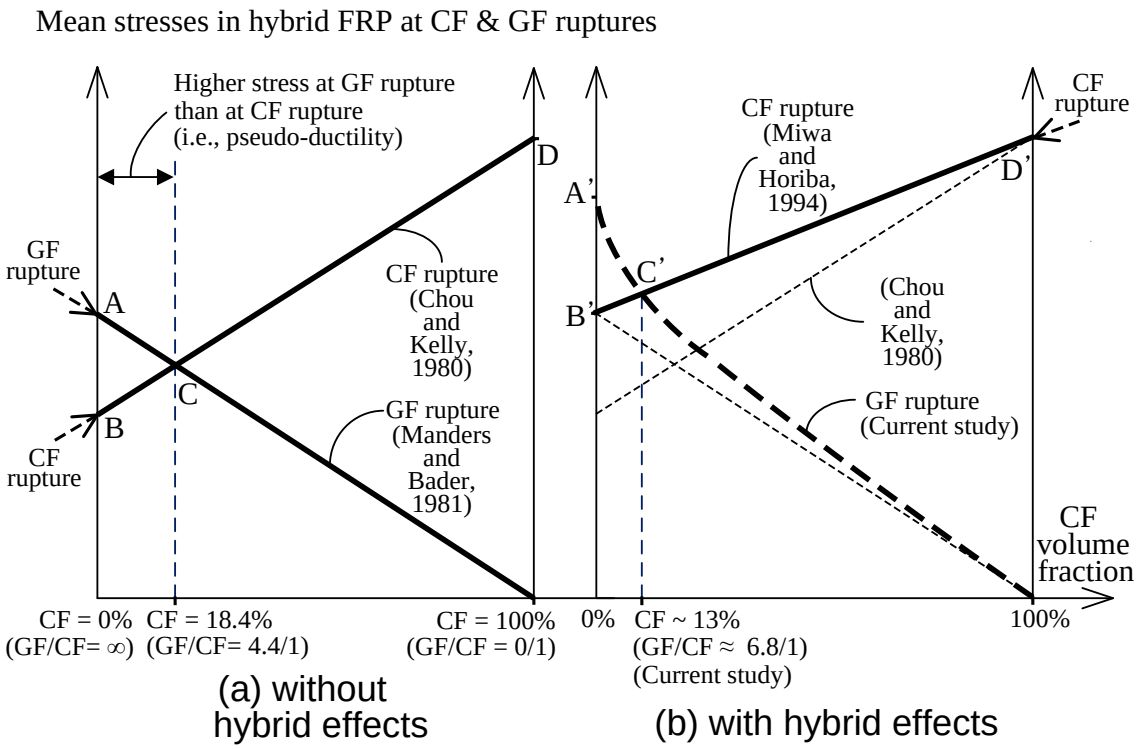

Figure 5 Theoretical Tensile Stress Models for Hybrid Carbon-Glass FRP (Scaled Based on the Measured Stresses from the Roving Tests or Sheet Tests)

Many researchers [1], [2], [13] have observed the hybrid effect in terms of the increased stress and strain of hybrid carbon-glass composites at CF rupture. Manders and Bader [2] reported approximately 50% increase in stress at CF rupture, and Miwa and Horiba [13] suggested the rule of "hybrid" mixtures as follows:

$$f_{u\_C\_HF} = \frac{f_{u\_CF}(V_{CF}) + f_{u\_GF}(V_{GF})}{(V_{CF} + V_{GF})} \quad (1)$$

where $f_{u\_C\_HF}$ is the mean stress of hybrid FRP at CF rupture (i.e., line B'-C' in Figure 5(b)), V_{CF} is the CF volume and V_{GF} is the GF volume. The increased ultimate stress of hybrid FRP at GF rupture (e.g., line A'-C' in Figure 5(b)) has not been clearly identified; thus, an experiment is attempted in this study. A modified tensile stress trend for hybrid carbon-glass FRP is introduced as shown in Figure 5(b) based on the hybrid sheet tensile tests and the previous research [2], [13].

Uni-axial hybrid carbon-glass FRP sheets were fabricated with (GF/CF) ratio of (8.8/1), which lies in the A-C or A'-C' regions. Figure 2(b) shows a picture of the fabricated hybrid sheet with cross-sectional area of about 0.027 in^2 (17.4 mm^2), with CF of 0.024 in^2 (15.6 mm^2) and GF of 0.003 in^2 (1.8 mm^2), being tested in accordance with CSA S806-02 [14]. A Universal Test Machine with a capacity of 270 kips (1200 kN) was used to test the sheets. Strains were monitored using both strain gauges and Linear Variable Displacement Transducers (LVDT). Tensile stress-strain relations of 2 samples and that of steel are plotted in Figure 3(b), where the LVDT data were used to determine strains.

Test results indicate that CF ruptured at about 0.014 strain and 122.4 ksi (844.4 MPa) stress. This stress is very close to the analytical value of 122.4 ksi (844.4 MPa) estimated from Equation (1). After CF rupture, the hybrid strength was regained and increased further until the ultimate failure of GF at about 0.022 strain, greater than the measured ultimate strain of the GF roving (ε_{u_GF} = 0.0176). The mean ultimate stress for the 3 samples was 158.6 ksi (1,094 MPa), about 38% higher than f_{u_GF} (= 114.8 psi; 792 MPa). Although the test results are limited, judging from those samples, the increased ultimate stress and strain are likely due to the sequential fiber failure and the associated

hybrid effect (see the curved line in Figure 5(b)). Also, the average strain of 0.014 and stress of 122.4 ksi (844.4 MPa) at CF rupture of hybrid FRP are substantially greater than the values of ε_{u_CF} (= 0.0112) and (ε_{u_CF} x E_{GF} = 73 ksi; 504 MPa), again owing to the hybrid effect. This observation simply verifies the previous research [2], [13], where the hybrid effect is defined as increased stress and strain at CF rupture in a hybrid.

3. FLEXURAL TESTS OF CONCRETE BEAMS STRENGTHENED WITH FRP SHEETS

This chapter presents flexural tests of plain concrete beams strengthened by a variety of combinations of fibers (e.g., varying [GF/CF] volume ratios and epoxy-to-fiber volume ratios), as well as their results.

3.1 PLAIN CONCRETE BEAMS STRENGTHENED WITH FRP ROVING

In order to determine an optimal glass-to-carbon volume ratio such that sufficient pseudo-ductility can be obtained, plain concrete beams strengthened with different combinations of CF and GF were tested under four-point loading (Table 2). The beam size was 3.5 x 3.5 x 31.5 in. (90 x 90 x 800 mm). Fiber rovings were attached on the tension side of plain concrete beams. The distance between a support and a loading point on each side of the beam was 11.8 in. (300 mm), and the distance between two loading points was 3.9 in. (100 mm). The beams with either CF or GF were also tested for the comparison purpose. The amount of fibers was controlled by changing the number of the fiber roving. Also, limiting the fiber amount was attempted so as not to make the beam over-reinforced. The epoxy-to-fiber volume ratio was varied from 1 to 1.5 to 2. For the hybridized H-series (see Table 2), either CF or GF rovings were first mounted on the concrete, and the other fiber rovings were attached on top of the first fiber rovings. As indicated in Table 2, three different GF/CF ratios (4.9/1, 6.8/1, and 9.1/1) were tested. Each specimen configuration is provided in Table 2. In order to prevent bond failure, the FRP sheets were anchored at its ends by composite anchorage (use of FRP bars, epoxy adhesives and reaction steel plates; see Figure 6).

Table 2 Measured Test Data for Plain Concrete Beams

	Fibers	A_{CF} (mm^2)	A_{GF} (mm^2)	(GF/CF) by volume	ρ_{HF}	Epoxy/Fiber by volume	P_{cr} (kN)	P_{max} (kN)	Δ_{mid} at P_{max} (mm)	Failure mode
C-1	CF	3.55	0	∞	0.00044	2	4.92	5.8	18	FR
G-1	GF	0	17.3	0/1	0.00214	2	5.4	12.4	21.8	FR
H-1-4.9/1	GF+CF	3.55	17.3	4.9/1	0.00257	2	5.58	15.1	18	FR
C-2	CF	5.33	0	∞	0.00066	2	4.38	8.7	19.4	FR
G-2	GF	0	26	0/1	0.00321	2	5.46	21.4	28.3	FR
H-2-4.9/1	GF+CF	5.33	26	4.9/1	0.00387	2	7.38	16.2	19	CC
C-3(a)	CF	2.66	0	∞	0.00033	1.5	3.72	11.6	11.6	FR
C-3(b)	CF	2.66	0	∞	0.00033	1.5	3.66	3.2	13.5	FR
G-3(a)	GF	0	18.2	0/1	0.00225	1.5	5.22	10.6	15.8	FR
G-3(b)	GF	0	18.2	0/1	0.00225	1.5	4.68	13.1	22.7	FR
H-3-6.8/1(a)	GF+CF	2.66	18.2	6.8/1	0.00258	1.5	4	14.3	17.8	FR
H-3-6.8/1(b)	CF+GF	2.66	18.2	6.8/1	0.00258	1.5	4.68	14.9	21.9	FR
H-4-6.8/1(c)	GF+CF	1.78	12.1	6.8/1	0.00171	1.5	5.82	11.2	20.6	PD
H-4-6.8/1(d)	GF+CF	1.78	12.1	6.8/1	0.00171	1	3.3	9.06	17.9	FR
H-5-9.1/1(a)	GF+CF	1.33	12.1	9.1/1	0.00166	1.5	4.38	7.32	14.2	PD
H-5-9.1/1(b)	GF+CF	1.33	12.1	9.1/1	0.00166	1	4.38	8.46	22	PD

Note: CF = Carbon Fibers; GF = Glass Fibers;
GF+CF = GF is first applied, followed by CF; GF+CF = GF is first applied, followed by CF;
A_{CF} = cross-sectional area of CF rovings; A_{GF} = cross-sectional area of GF rovings
$\rho_{HF} = (A_{CF} + A_{GF}) / (bd)$, where b is the member width (= 3.54 in.; 90 mm), d is approximated as $0.9h$ (= 3.54 in.; 90 mm), and h is the member depth (= 3.94 in.; 100 mm);
P_{cr} = Applied load at concrete cracking; P_{max} = Applied maximum load; Δ_{mid} = Mid-span deflection at P_{max};
FR = Fiber Rupture; CC = Concrete Crushing; PD = Pseudo-Ductility
Conversion: 1 mm = 0.0394 in.; 1 mm^2 = 0.00155 in^2; 1 kN = 0.2248 kips

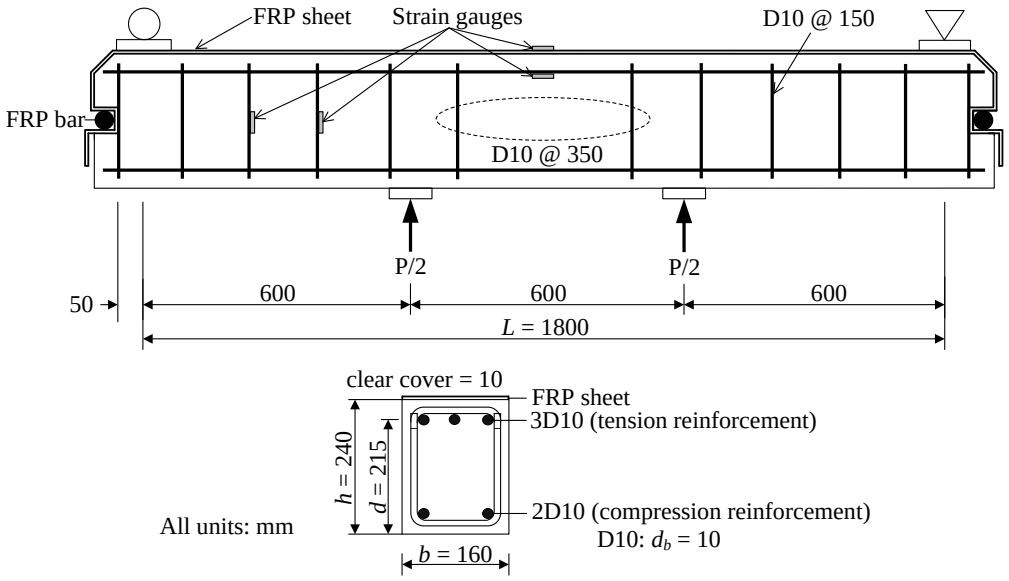

Figure 6 Test Specimen and Set-Up Details for Reinforced Concrete Beams Strengthened with FRP Sheets

Figure 7(a) compares load-displacement relations for C-1, G-1 and H-1-4.9/1. All beams failed in a relatively brittle manner due to the fiber rupture. The first peak at about 0.01 in. (0.25 mm) corresponds to concrete cracking (note that no reinforcing bars were provided). After the first peak, the beams sustained more loads until the first fiber ruptured. The displacement at ultimate failure of G-1 was the same as that at peak of H-1-4.9/1 after which the load capacity dropped, and the displacement at ultimate failure of C-1 was the same as that when carbon fibers in H-1-4.9/1 ruptured. The H-1-4.9/1 with a (GF/CF) ratio of (4.9/1) exhibited a substantial loss in load-carrying capacity after CF rupture, which occurred before GF rupture.

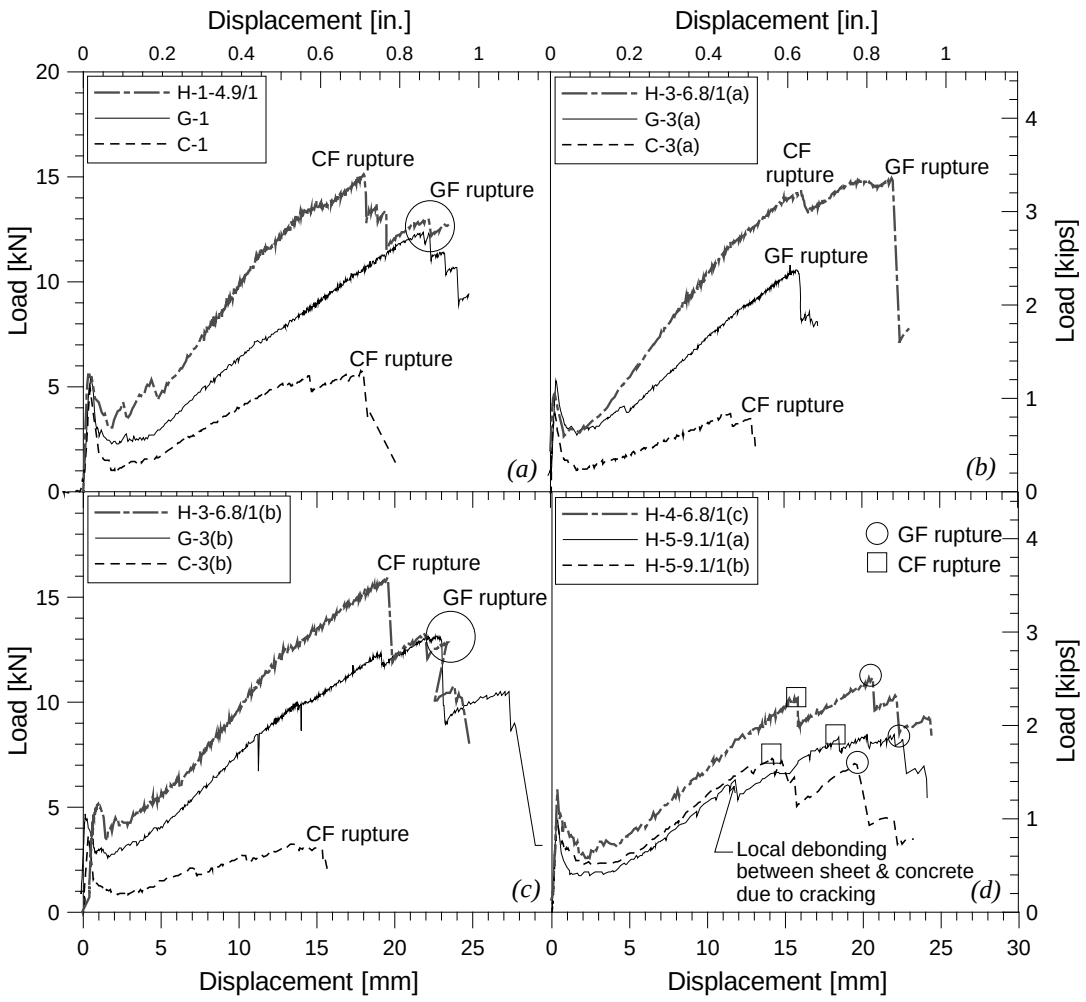

Figure 7 Measured Load versus Mid-Span Deflection Relations for Plain Concrete Beams

This indicates that the theoretical minimum ratio of (4.4/1), which is defined by Point C in Figure 5(a), is not sufficient to produce the pseudo-ductility (i.e., the load was maximum at CF rupture). Similar comparisons were made between C-2, G-2 and H-2-4.9/1, but with increased amounts of fibers (by 50% compared with 1-series). Due to over-reinforcing, H-2-4.9/1 failed in concrete crushing at the top of the beam.

The H-6.8/1-series (see Table 2) were reinforced with the hybrid FRP rovings with a (GF/CF = 6.8/1) ratio. The difference between H-3-6.8/1(a) and H-3-6.8/1(b) was the order of attachment of GF and CF fibers, and the difference between H-4-6.8/1(c) and H-4-6.8/1(d) was the different epoxy-to-concrete volume ratio. Although the ductility for all H-6.8/1-series specimens was improved over the H-4.9/1-series, only H-3-6.8/1(a) and H-4-6.8/1(c) behaved in a pseudo-ductile manner. It is notable that CF ruptures in H-3-6.8/1(a) and H-3-6.8/1(b) occurred at higher displacements than those of G-3(a) and C-3(b) or even G-3(a) (Figures 7(b) and 7(c)), likely due to the hybrid effect. For H-3-6.8/1(b), the post-peak behavior after CF rupture was almost the same as that of G-3(b). Overall, the ratio of (6.8/1) produced sufficient ductility. Note that this ratio lies left of Point C in Figure 5(a) and about at Point C' in Figure 5(b).

Both H-5-9.1/1 specimens with (GF/CF = 9.1/1) showed the pseudo-ductility. Particularly, the rather slowly loaded H-5-9.1/1(a) exhibited highly ductile behavior without strength degradation during sequential fiber ruptures. The H-5-9.1/1(b) subjected to slightly faster loading did not achieve increased load capacity after the first peak (when CF failed), but at least maintained the same strength at the second peak (when GF failed). Figure 7(d) indicates that the load slightly dropped at displacement of about 0.5 in. (12 mm) when flexural cracking occurred in the mid-span region and that at this instant, slippage between the concrete and fibers occurred due to the different concrete surface levels of each side (note that there were no reinforcing bars). Nevertheless, this debonding affected little on the overall behavior.

Based on the plain concrete beam tests, a ratio of (GF/CF) of (8.8/1) was selected for fabrication of uni-axial hybrid carbon-glass FRP sheets, and experimentally examined through large-scale testing of strengthened RC beams as detailed in the following section. In terms of the order of fiber attachment and the epoxy-to-concrete volume fraction, no recommendations are possible from this study due to the lack of evident data.

3.2 REINFORCED CONCRETE BEAMS STRENGTHENED WITH HYBRID FRP SHEETS

Flexural tests of a total of six under-reinforced concrete (RC) beams were carried out under four-point loads. As shown in Figure 6, 6.3 x 9.4 x 78.7 in. (160 x 240 x 2,000 mm) sized beams were used. Three tension and two compression bars with 0.4 in. (10 mm) diameter were provided. The loading points were selected such that a 23.6 in. (0.6 m) long constant moment region exists in the center of the beam with 71 in. (1.8 m) center-to-center span length. Two control specimens had no FRP sheets (RC-0(a), RC-0(b)), while the rest of the specimens were strengthened using 1-ply, 2-ply and 3-ply hybrid sheets (HF-1ply, HF-2ply and HF-3ply) and 1-ply carbon-only sheets (CF-1ply), respectively (Table 3). All sheets had a width of 5.5 in. (140 mm). Because the mid-span deflection of RC-0(a) was not measured, RC-0(b) with the same configuration was additionally tested. An epoxy-to-FRP sheet volume ratio of (1.5/1) was chosen for all specimens. As used for the plain concrete beam tests, the same anchorage system was applied for the RC beam tests to prevent debonding of the sheets from the concrete (see Figure 6).

Table 3 summarizes test results of loads, deflections and strains at different steps, ductility, and failure modes. Figures 8(a) and 8(b) depict load versus mid-span deflection relations, displaying a sequential series of failures of each material. As shown in Figure 8(a), while the failure modes for all specimens were flexure, the control specimen of RC-0(b) with bottom reinforcing ratio of 0.7% showed the highest degree of ductility (≈ 5). The specimen HF-1ply also underwent extensive GF rupture and exhibited pseudo-ductility. The displacement at ultimate (δ_u = 1.3 in.; 33 mm) was slightly less than δ_u of RC-0(b) (= 1.5 in.; 37 mm), but the strength of HF-1ply was kept higher than RC-0(b) until δ_u of RC-0(b). The maximum strength of HF-1ply was about 120% of the maximum of RC-0-series. The specimen CF-1ply began to fail at substantially lower displacement of 0.95 in. (24 mm) and exhibited ultimate failure at 1.3 in. (33 mm).

Table 3 Measured Test Data and Analytical Results for Reinforced Concrete Beams

	P_y (kN)	Δ_{mid_y} (kN)	P_{max} (kN)	Δ_{mid_y} at P_{max} (mm)	P_{fail} (kN)	Δ_{mid_fail} at P_{fail} (mm)	μ	Strain (%) @ failure			Failure Mode	M_{max} (kN-m)	M_n^* (kN-m)	M_n^{**} (kN-m)	M_n^{***} (kN-m)	M_r^* (kN-m)	M_r^{**} (kN-m)
								ε_s	ε_c	ε_f							
(1)	(2)	(3)	(4)	(5)	(6)	(7)	(8)	(9)	(10)	(11)	(12)	(13)	(14)	(15)	(16)	(17)	(18)
RC-0(a)	NA	NA	89.1	NA	78.6	NA	NA	> 0.76	NA	NA	CC	28.6	20.4	20.4	25.6	17.3	17.3
RC-0(b)	79.6	7.48	90.9	34.7	86.3	37.0	5	> 0.78	0.45	NA	CC	29.1	20.4	20.4	25.6	17.3	17.3
HF-1ply	88.9	7.7	110	29.4	95.7	36.8	4.8	> 1.23	0.49	NA	GF	34.9	25.9	25.9	33.1	22.6	21.4
HF-2ply	96.5	8.13	126	26.1	106	33.4	4.1	> 0.9	0.39	1.19	GF	39.7	27.8	31.3	40.5	24.1	24.8
HF-3ply	NA	NA	151	26.7	148	30.9	NA	> 1.1	0.26	0.97	GF–A	47.2	29.2	36.0	47.8	25.2	27.3
CF-1ply	91.9	7.46	103	18.1	83.3	32.8	4.4	> 2.17	0.31	0.76	CF	32.8	25.1	24.9	30.1	22.1	20.6

Note: NA = Not Available; RC = RC beam without fibers;
HF-1ply = 1 ply of Hybrid FRP sheet, with A_{CF} = 0.006 in^2 (3.55 mm^2) and A_{GF} = 0.048 in^2 (31.2 mm^2);
HF-2ply = 2 plies of Hybrid FRP sheets, with A_{CF} = 0.011 in^2 (7.1 mm^2) and A_{GF} = 0.097 in^2 (62.4 mm^2);
HF-3ply = 3 plies of Hybrid FRP sheets, with A_{CF} = 0.017 in^2 (10.65 mm^2) and A_{GF} = 0.145 in^2 (93.6 mm^2);
CF-1ply = 1 ply of Carbon FRP sheets, with A_{CF} = 0.0248 in^2 (16 mm^2);
y = at yielding; *max* = at maximum; *fail* = at failure; *P* = applied load; Δ_{mid} = Mid-span deflection; $\mu = (\Delta_{mid\_fail} / \Delta_{mid\_y})$;
ε_s = strains in steel (from SG); ε_c = strains in concrete on the compression face of the beam (from SG);
ε_f = strains in FRP (from SG); SG = Strain Gauges;
CC = Concrete Crushing; GF = GF rupture; A = Anchorage failure; CF = CF rupture;
M_{max} = Moment at P_{max}, including self-weight-induced moment; M_n = Nominal moment strength; M_r = Factored resisting moment;
*: based on ACI 440.2R-08 and the model of Figure 9(a);
**: based on ISIS Canada Design Manual No. 4 and the model of Figure 9(a);
***: based on ISIS Canada Design Manual No. 4, the model of Figure 9(b), measured ultimate steel strain (= 559 MPa; 81 ksi), α_1 = 1, and concrete crushing strain (ε_{cu}) of 0.005;
Conversion: 1 kN = 0.2248 kips; 1 mm = 0.0394 in.; 1 kN-m = 8.85 kips-in.

The flexural strengths of HF-2ply and HF-3ply were increased due to the increased amounts of FRP by about 15% and 35% over HF-1ply, respectively (see Column (13) of Table 3); however, HF-2ply and HF-3ply failed at smaller displacements. The brittle failure mode for HF-2ply is likely due to epoxy bond failure triggered by the initiation of GF rupture (observed and confirmed via video). For HF-3ply, FRP anchorage failure at the end vertical face of the beam was observed prior to the initiation of GF rupture.

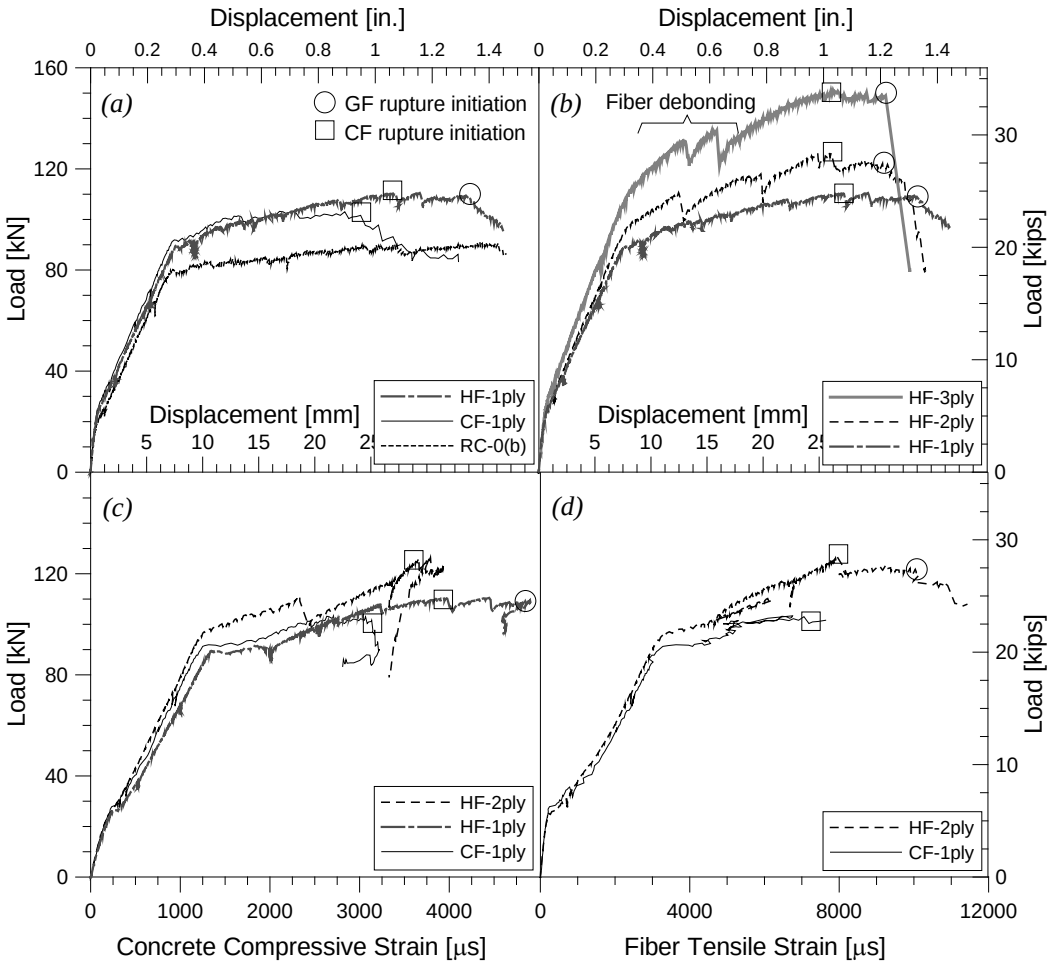

Figure 8 Measured Load versus Mid-Span Deflection or Strain Relations for Reinforced Concrete Beams

Figures 8(c) and 8(d) depict load versus concrete compression strain or tension FRP strain relations. The order of the magnitude of concrete compression strains at section failure was HF-1ply > HF-2ply > CF, which is consistent with the observation. The CF failed due to extensive CF rupture with concrete deterioration, whereas HF-1ply exhibited extensive CF and GF ruptures. The neutral axis location which was apparently predicted from the crack formation supported that CF failed prior to the concrete crushing. For HF-2ply, less ductile failure (compared with HF-1ply) was noted after a moderate degree of GF rupture, although the degree of steel yielding was extensive. The observed delamination is also evidenced by the rapid post-peak degrading curves in Figure 8(a) and 8(c), where modest concrete strain changes of HF-2ply are shown even at failure.

In Figure 8(d), the FRP strain at failure of CF-1ply corresponded to that at CF failure of HF-2ply, revealing that the higher displacement capacity of HF-2ply resulted from the sequential failures of the hybrid sheet and that the fiber rupture was the main cause of CF-1ply failure. The strain gauge data of CF-1ply and HF-2ply at fiber ruptures are somewhat smaller than ε_{u_CF}, ε_{u_GF} or ε_{u_HF} of the rovings (or the sheet), which were monitored from LVDTs or those of the Universal Test Machine.

This Page is Intentionally Blank

4. FLEXURAL STRENGTH PREDICTIONS OF RC BEAMS REPAIRED WITH FRP SHEETS

In this chapter, flexural strengths of the tested beams are predicted using two different approaches outlined below, and compared with the corresponding test data.

4.1 PREDICTIONS BASED ON ACI 440.2R-08

Although the procedure described in ACI 440.2R-08 [6] generally utilizes the strain compatibility and equilibrium, it empirically accounts for bond deterioration (e.g., intermediate crack-induced debonding or cover delamination initiated at the sheet end due to curtailment) by using a reduction factor (ψ_f) and considering the FRP effective strain (ε_{fe}). The value of ε_{fe} is limited to the debonding strain of ε_{fd} as follows:

$$\boldsymbol{\varepsilon_{fe} \leq \left[\varepsilon_{fd}\left(= 0.41\sqrt{\frac{f'_c}{nE_f t_f}}\ \textbf{in SI units or}\ 0.083\sqrt{\frac{f'_c}{nE_f t_f}}\ \textbf{in in.}-\textbf{lb units}\right) \leq 0.9\varepsilon_{fu}\right]} \quad (2)$$

where n is the number of plies of FRP sheets, E_f is the elastic modulus of FRP, t_f is the nominal thickness of one FRP ply (= 0.01 in. or 0.25 mm in this study), and ε_{fu} is the design ultimate strain of FRP (= f_{u_GF}/A_{GF} for HF-series, as shown in Figure 9(a)). It is recommended that t_f be obtained based on the materials' mechanical properties, not by directly measuring, as noted earlier.

In this study, it turns out that HF-1ply, HF-2ply and HF-3ply have ε_{fe} values equal to ε_{fd} in Equation (2), which is less than $0.9\varepsilon_{fu}$ at section failure, and CF-1ply has ε_{fe} equal to $0.9\varepsilon_{fu}$ (= 0.9 x 0.00112 = 0.01). The ψ_f factor of 0.85 is applied to account for uncertainties inherent in FRP as follows:

$$\boldsymbol{M_r = \phi M_n = \phi \left[A_s f_s \left(\frac{d - \beta_1 c}{2} \right) + (\psi_f = 0.85) A_f f_{fe} \left(h - \frac{\beta_1 c}{2} \right) \right]} \quad (3)$$

where the strength reduction factor of ϕ and the Whitney stress block depth factor of β_1 are in accordance with ACI 318-08 [15] (Sections 9.3.2 and 10.2.7.3, respectively), A_s and f_s are the cross-sectional area and stress of the steel at section failure, respectively, d is the effective depth, A_f is the cross-sectional area of FRP (= A_{GF} after CF rupture), f_{fe} is the effective stress (= $\varepsilon_{fe}E_f$) in FRP, E_f is the elastic modulus of FRP, and h is the member depth. As noted, M_n includes the ψ_f factor effects; however, no environmental reduction factors for exposure conditions (C_E = 1) and no initial strains prior to FRP repair are applied.

4.2 PREDICTIONS BASED ON ISIS CANADA DESIGN MANUAL NO. 4

The procedure described in ISIS Canada Design Manual No. 4 [7] utilizes the concept of strain compatibility and perfect bonding between FRP/steel and concrete to determine strains of FRP sheets, assuming that the ultimate compressive strain of concrete (ε_{cu}) is 0.0035. Other assumptions include no strain hardening of steel bars and the equivalent concrete stress block defined by CSA-A23.3-94 [16]; thus, the compression force of a rectangular section at ultimate is equal to $(\alpha_1 f'_c)(\beta_1 c)b$, where f'_c is the specified concrete strength, α_1 = [0.85 – 0.0015(f'_c in MPa) ≥ 0.67], β_1 = [0.97 – 0.0025(f'_c in MPa) ≥ 0.67], c is the neutral axis depth at ultimate, and b is the beam width. In the prediction, as-measured strength was used.

Several different failure scenarios are possible for RC beams with hybrid FRP sheets, and the scenarios with the presence of steel bar yielding (but without debonding of FRP) include: (i) concrete crushing without fiber ruptures; (ii) CF rupture, followed by concrete crushing without GF rupture; and (iii) GF rupture, following CF rupture without concrete crushing. On the other hand, CF-1ply fails in Scenario (i) or (ii). The factored resisting moment (M_r) and nominal moment strength (M_n) of HF specimens are calculated using the strain compatibility and equilibrium in Equation (4) with and without strength reduction factors (ϕ), and also considering the above three scenarios.

$$\left[\boldsymbol{C_s}\left(= \boldsymbol{\phi_s f'_s A'_s} \le \boldsymbol{\phi_s f_y A'_s}\right) + \boldsymbol{C_c}\left(= \boldsymbol{\phi_c \beta_1 f'_c c b}\right)\right] = \left[\boldsymbol{T_s}\left(= \boldsymbol{\phi_s f_y A_s}\right) + \boldsymbol{T_{frp}}\left(= \boldsymbol{\phi_{frp} \phi_{frpe} F_{frp}}\right)\right] \quad (4)$$

where f'_s is the stress in compression steel bars at section failure, A'_s is the cross-sectional area of compression steel bars, f_y is the specified yield stress of steel (but measured values were used in this section), A_s is the cross-sectional area of tension steel bars, T_{frp} is the factored tensile force in FRP, and F_{frp} is the tensile force in FRP at section failure. In Equation (4), different strength reduction factors are applied for each material or force applied to each material (versus a strength reduction factor corresponding to bending moment) as follows: ϕ_c = 0.6 for concrete; ϕ_s = 0.85 for steel bars; and ϕ_{frp} = 0.75 for FRP sheets. No environmental reduction factors for exposure conditions are applied (ϕ_{frpe} = 1). The initial strains due to gravity loads prior to FRP retrofitting are all zero because the FRP sheets were attached and then the beams were placed on the test set-up. In the process, the tensile force (F_{frp}) carried by the hybrid FRP sheet at section failure needs to be carefully determined, as detailed in the following subsection.

4.2.1 Analytical Force-Strain Relationship for Hybrid Carbon-Glass FRP Sheets

In this study, two force-strain relationships for hybrid FRP sheets are proposed as shown in Figure 9. The first one (Figure 9(a)) is the model with no hybrid effect,

whereas the second one (Figure 9(b)) is the model with the consideration of the hybrid effect, where the increased stress and strain at fiber failures are characterized when hybridization is used.

The analytical force path of the first model follows from Points [1] to [5] in Figure 9(a), depending upon the corresponding strain in the hybrid FRP sheet. The tension force is taken as ($\varepsilon_f E_{HF} A_{HF}$) prior to CF rupture, where ε_f is the strain (variable), and A_{HF} and E_{HF} are the cross-sectional area and elastic modulus of hybrid FRP sheets prior to CF rupture, respectively. The weighted mean elastic modulus of E_{HF} is estimated as:

$$\boldsymbol{E_{HF}} = \frac{\boldsymbol{E_{CF}A_{CF}+E_{GF}A_{GF}}}{\boldsymbol{A_{CF}+A_{GF}}} \quad (5)$$

Once the CF rupture occurs at ε_{u_CF} that is calculated as (f_{u_CF}/E_{HF}) (Point [2]), the tensile force in the FRP sheet drops to Point [3] and the cross-sectional area of the sheet becomes (A_{GF}) from ($A_{CF} + A_{GF}$). The strains of ε_2 and ε_3 are simply the same in the model. For the path from Points [3] to [5], the force is almost the same as that of the FRP sheets with only glass fibers. Thus, the force is taken as ($\varepsilon_f E_{GF} A_{GF}$). Finally, the

measured ultimate stress of f_{u_GF} is used in the model to define Point [5] (see Table 1).

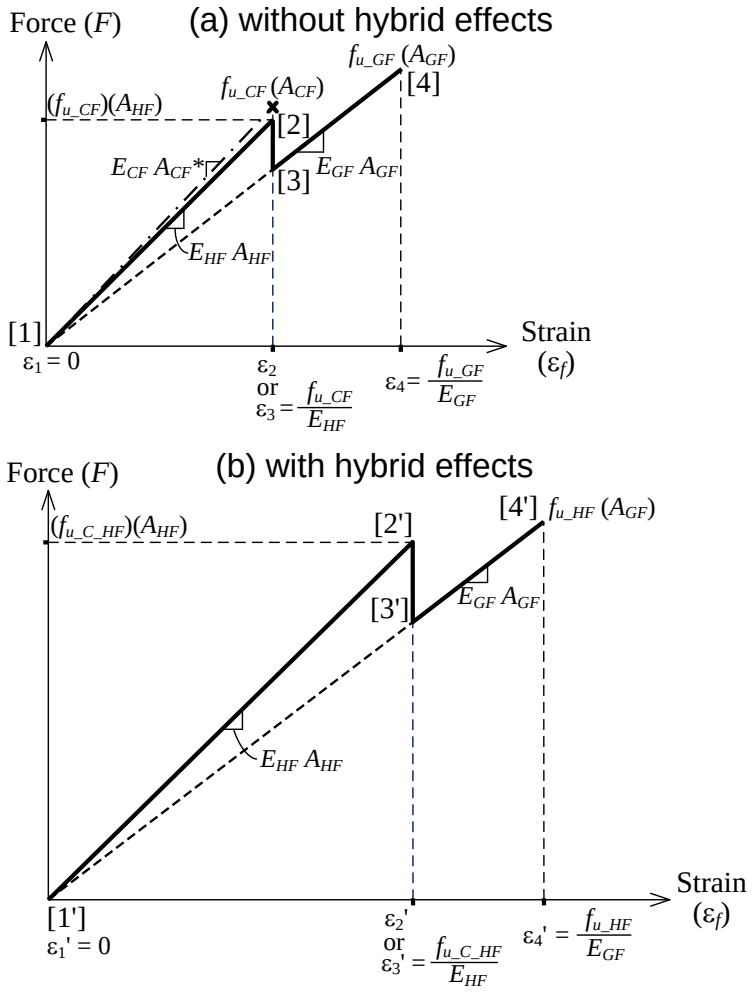

Note: A_{CF}* = 16 mm^2 = cross-sectional area of CF used for CF-1ply
Dash-dot line represents force-strain relationship for CF used for CF-1ply
$f_{u\_C\_HF}$ = increased stress at CF rupture of hybrid FRP

Figure 9 Proposed Analytical Force-Strain Relationship for Hybrid FRP Sheets [Scaled Based on the Measured Data from the Roving Tests (f_{u_CF}, f_{u_GF}, E_{u_CF} and E_{u_GF}) and Sheet Tests (f_{u_HF}); see Table 1, Equations (1) and (3)]

The analytical force path of the second model follows from Points [1'] to [4'] in Figure 9(b), addressing the hybrid effect of carbon-glass composites. The stiffnesses are the same as that in the first model; however, the carbon fiber rupture occurs at the larger strain of ($f_{u\_C\_HF}/E_{HF}$) defined as $\varepsilon_{u\_C\_HF}$, and the glass fiber also at the larger strain of (f_{u_HF}/E_{HF}), where $f_{u\_C\_HF}$ is estimated based on the rule of hybrid mixtures as noted earlier in Equation (1), and f_{u_HF} is estimated from the tensile sheet tests.

For all specimens, $\varepsilon_{u\_C\_HF}$ (ε_2 or ε_3) is calculated as 0.0162 (= 842/52,000), slightly greater than the measured average strain (0.014) at CF rupture of three hybrid FRP sheets. Also, note that ε'_4 (= f_{u_HF}/E_{GF} = 0.0243) in Figure 9(b) is slightly larger the measured ε_{u_HF} (= 0.022). As indicated in Figure 9, the proposed analytical models include only the following variables: A_{CF}, A_{GF}, E_{CF}, E_{GF}, f_{u_CF}, f_{u_GF} and/or f_{u_HF}.

4.3 FLEXURAL STRENGTH PREDICTIONS

Based on the discussions in the preceding sections, flexural strengths of reinforced concrete beams strengthened using hybrid FRP sheets were obtained, along with those of RC-0 and CF-1ply. Table 3 compares the measured peak moments to the predicted strengths of M_n and M_r, both of which were calculated using as-measured material properties. The measured values in Table 3 also account for self-weight-induced moments. The force-strain model described in Figure 9(a) was used. Both ACI 440 [6] and ISIS Canada [7] procedures give very conservative estimates of M_n and M_r for HF specimens compared with the test results by margins of 35% and 63% on average, respectively.

The underestimation of M_n is likely due to the absence of strain hardening in steel modeling and lack of adequate consideration of hybrid effects and confined concrete. If the model with consideration of hybrid effects is incorporated as shown in Figure 9(b), along with increased strength and/or ductility of steel (i.e., use of f_u = 81 ksi; 559 MPa instead of f_y = 64.7 ksi; 446.5 MPa) and confined concrete (e.g., α_1 = 1 and ε_{cu} = 0.005, as recommended by Tomii [17]), the predictions are very good with an average 2% difference (see Table 3). The steel strain hardening appeared to occur given that the predictions for the RC-0-series and CF-1ply in Column (16) of Table 3 are also reasonable. It is noted that the concrete strain was achieved up to 0.005 without crushing for HF-1ply that failed in GF rupture (Figure 8(c)). The degree of conservativeness that the ACI 440 method introduces is similar to that of the ISIS Canada method. The results in this paragraph demonstrate the presence of the hybrid effect that was also observed during the sheet tensile tests.

Column (15) of Table 3 indicates that the predicted strength of HF-1ply is slightly higher than that of CF-1ply, as intended at the design stage. The test results showed a similar trend (Table 3, Column (13); and Figure 8). The ductility and cost effectiveness, however, are substantially higher for HF-1ply than CF-1ply. Assuming that the costs per unit weight of carbon and glass filaments are $35/kg (or $15.9/lb) and $2/kg ($0.9/lb), respectively, the total cost of FRP sheets needed for HF-1ply and CF-1ply would be $382 and $1,008, respectively. This is, no doubt, an important aspect of value engineering.

4.4 MAXIMUM AMOUNT OF HYBRID FRP SHEETS FOR DUCTILE BEHAVIOR OF RC BEAMS

The plain beam tests indicated that the optimal ratio of (GF/CF) was (8.8/1), with the ratio required to be at least (6.8/1) to produce the pseudo-ductility. In this section, maximum absolute amount of hybrid carbon-glass FRP sheets to ensure ductile behavior of a reinforced concrete beam is investigated.

Based on the procedure used to obtain M_n values in Column (16) of Table 3 (e.g., use of the model in Figure 9(b)) and the following equilibrium, the maximum amount of hybrid FRP sheets (or $\rho_{HF\_max} = A_{HF\_max}/bd$) that causes the beam to fail by GF rupture (i.e., simultaneous failures of concrete and glass fibers) can be determined as 0.2 in^2 (130.7 mm^2) or ρ_{HF_max} of 0.0038 for the tested beam.

$$\left[\boldsymbol{E_s\varepsilon'_sA'_s}\left(\leq \boldsymbol{f_yA'_s}\right) + (\boldsymbol{\alpha_1 f'_c})(\boldsymbol{\beta_1 c})\boldsymbol{b}\right] = \left[\boldsymbol{f_yA_s} + \boldsymbol{A_{GF\_max}f_{u\_HF}}\right] \quad (6)$$

As the concrete is well confined, the extreme concrete compression strain (ε_{cu}) is assumed to be 0.005, 1991), and be reached when the ultimate hybrid FRP strain (ε_{fu}) of (f_{u_HF}/E_{GF}) (i.e., ε_4' in Figure 9(b)) is reached. In Equation (6), c and ε_s' are computed as [(h)(ε_{cu})/(ε_{cu} + ε_{fu})] and [(ε_{cu})(c – d')/(c)], respectively, at the balanced failure condition, d' is the effective depth of compression reinforcement (from the compression concrete face), and A_{GF_max} is the maximum amount of GF in hybrid FRP that results in simultaneous failures of concrete and glass fibers in hybrid FRP. Once A_{GF_max} is obtained from Equation (6), the hybrid FRP sheet area (A_{HF_max}) is then simply calculated as A_{GF_max} times [(V_{GF} + V_{CF})/V_{GF}], that is, A_{HF_max} = (A_{GF_max}) x (9.8/8.8) for the ratio of (GF/CF = 8.8/1).

Under this balanced failure condition, steel tension bars would yield substantially and substantial ductility would be maintained in the hybrid FRP beyond CF rupture. The flexural strength (M_n) with ρ_{HF_max} would be 406.3 in.-kips (45.9 kN-m), about 125% larger than the same beam without FRP sheets. It should be noted that the analytical maximum FRP ratio (ρ_{HF_max}) of 0.0027 is coupled with the tension and compression reinforcing ratios ($\rho_{tension}$ and ρ_{comp}) of 0.0069 and 0.0046, respectively, and is valid only for the ratio of (GF/CF = 8.8/1), as noted in Equation (6). The value of (ρ_{HF_max} = 0.0027) is quite consistent with the experimental results, which indicated that HF-3ply with (ρ_{HF} = 0.003) exhibited a low degree of GF rupture just prior to anchorage/epoxy failure.

A similar strain compatibility section analysis was performed for different reinforcing ratios and (GF/CF) ratios using Equation (6). The same beam dimension was used for the analysis. The proposed force-strain model shown in Figure 9(b) was utilized to determine ρ_{HF_max}, along with the values obtained from Equations (1) and (2). Results show that the sensitivity of ρ_{HF_max} to steel reinforcing ratio is very high, whilst the impact of the (GF/CF) ratio is minimal. For instance, ρ_{HF_max} is only 0.0016 for a beam with ($\rho_{tension}$ = 0.009) and (ρ_{comp} = 0.0046) but the same other conditions as the tested beam. For a beam with both ($\rho_{tension}$ and ρ_{comp}) of 0 (assuming that all the bars corrode and rupture), ρ_{HF_max} is 0.005, and M_n with ρ_{HF_max} of 0.005 is about 90% of that of the un-strengthened original beam (RC-0).

The results from the analysis herein are important given that it is necessary to achieve both strength increase and pseudo-ductility of a retrofitted beam. Ideally, the hybrid FRP sheet is most useful to strengthen lightly reinforced rectangular members (with little compression reinforcement) and T-beams. It is recommended to use the hybrid FRP ratio (ρ_{HF}) not more than ρ_{HF_max}, or to identify the potential failure mechanism (e.g., concrete crushing before or after CF rupture). The use of hybrid FRP even with ρ_{HF} larger than ρ_{HF_max} is still useful, as its cost effectiveness and the hybrid effect in terms of increased stress at CF rupture would be beneficial.

In this section, the flexural strength of strengthened beams was evaluated for various reinforcing configurations of steel bars and FRP. The strain compatibility that was adopted in the analysis is valid when the epoxy adhesive has an ultimate strain on the order of 0.03 or 0.04, substantially greater than ε_{u_HF} (= 0.022). That was not the case for the epoxy used in this study (0.0197 < 0.022), and thus de-lamination between the sheets or at the beam end was observed.

This Page is Intentionally Blank

5. CONCLUSIONS OF PART I

The analytical and experimental study consists of material tests, structural tests, bond tests, and evaluation of the ACI 440 and ISIS documents. The results of the current study reveal that the volumetric ratio between glass and carbon fibers that exhibits pseudo-ductile behavior is (6.8/1) or greater. Based on the research, two design force-strain relations are also proposed for hybrid carbon-glass fiber-reinforced polymer sheets, with and without consideration of hybrid effects. Both the ACI 440 and ISIS methods in connection with the proposed force-strain relations give conservative predictions of flexural strengths of reinforced concrete beams strengthened using the hybrid FRP sheets, if no environmental effects are involved.

The beams strengthened using hybrid FRP sheets with the carbon-to-glass ratio of (8.8/1) exhibited higher peak loads than the un-strengthened beams by about 20%, sustained peak loads without degradation after the peak (up to ductility of about 5), and demonstrated pseudo-ductile behavior. The load-displacement relations of the beams strengthened using multiple layers of hybrid sheets indicated a reduction in flexural ductility, likely due to the bond deficiency which could be improved by using epoxy adhesives with a failure strain of at least 0.025 (possibly 0.04).

The maximum absolute amount of hybrid FRP sheets to ensure ductile behavior of a reinforced concrete beam needs to be considered; this figure is sensitive to steel amount (e.g., maximum hybrid FRP ratio = 0.0027 for the tested beam with tension and compression reinforcing ratios of 0.0069 and 0.0046, respectively). Also, the actual material properties of confined concrete, steel and FRP sheets, with the consideration of hybrid effects, can be accounted for to achieve better quantitative prediction of the capacity.

This Page is Intentionally Blank

PART II

6. INTRODUCTION TO PART II

Since the late 1980's fiber-reinforced polymer (FRP) sheets or wraps have been used to replace corrosion-vulnerable steel plates in repair applications. FRP sheets offer the advantages of light weight, high strength, low cost, and constructability and durability (non-corrosiveness). Despite the expensive cost relative to glass fibers (GF), carbon fibers (CF) and carbon FRP sheets/plates have been primarily used for repair and retrofit. This is mainly due to the fact that CF has a high elastic modulus and high ultimate strength (see Figure 10). GF is also popular, particularly for column jacketing (confining) retrofit, as it only costs about 5 to 10% as much as CF. GF has much less ultimate stress and very low elastic modulus (only about a quarter of that of steel), but very large ductility (Figure 10). It is noted that aramid fibers (AF) have both very large ductility and relatively high elastic modulus (Figure 10); however, because AF is as costly as CF, little economic advantage may be gained from the use of AF.

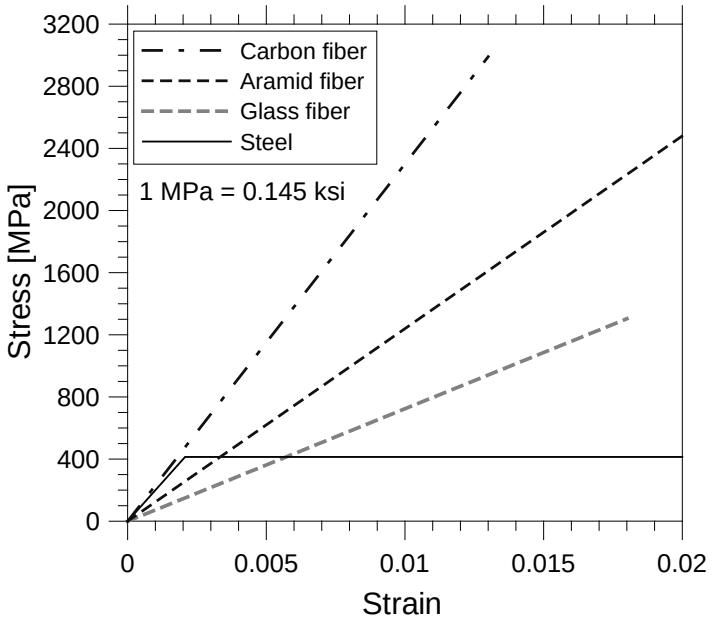

Figure 10 Comparison of Young's Moduli of Steel and Carbon, Aramid and Glass Fibers.

Brittleness is a major drawback of all these fibers (CF, AF and GF), since they have no yielding point and associated nonlinear behavior (Figure 10). To improve the ductility of the fibers, a number of composite material science investigations have been conducted on hybrid fibrous composites (e.g., [1], [2], [12], [13], [18], [19], [20], [21]). Applications of hybrid FRP composites, such as hybrid FRP bars and sheets combined with concrete, have been studied by several researchers (e.g., [3], [5], [22]). The primary purpose of these civil engineering applications was to achieve “pseudo-ductility” similar to the ductile response of nonlinear steel materials. Pseudo-ductility can be defined by the writers as when, after the first fiber failure (first drop in load), the load carrying capacity is recovered or improved as the remaining fibers elongate. Pseudo-ductility is also desirable because clear sound warning is produced during the first fiber failure, which indicates distress and the possible impending failure of structures.

The secondary purpose of hybrid FRP composites in civil engineering applications might be to actively utilize the so-called “hybrid effects.” Marom et al. [20] defined the hybrid effects as the deviation of the behavior of a hybrid composite from the rule of mixtures, while Manders and Bader [2] simply defined it as the difference in behavior between a fiber in a hybrid composite and in a non-hybrid composite. Both positive and negative hybrid effects are possible; the effects are deemed positive when mechanical properties are above the prediction based on the rule of mixtures and vice versa for negative effects. It is extremely difficult to theoretically predict the hybrid effects and mechanical properties of hybrid fibrous composites, which are known to depend on the volumetric ratio of each fiber component, bonding property between the components, and elastic moduli of the fibers or their ratio [21]. This is mainly due to the unavoidable uncertainty of the bonding property. Also, the size effect is involved. In civil engineering applications, hybrid FRP sheets or plates consisting of fiber rovings (strands) would be practical and feasible. A high-strength carbon fiber (CF) roving is typically made of about 12,000 filaments (12K) or multiples of 12,000 filaments (e.g., 24K or 48K), while an E-glass fiber (GF) roving is made of 1,200tex, 2200tex or multiple of 2,200tex, where 1tex is 1,000 m/g (or 459,920 yd/lb). Thus, some findings from previous research on a micro-composite or a composite made of a fraction of different fibers embedded in the

composite matrix (i.e., in the fiber roving or strand) may not be applicable to the hybrid FRP sheets that are focused on infrastructure repair or other civil engineering applications.

When the hybrid carbon-glass FRP sheet is subjected to tension, the CF with high elastic modulus and low ultimate strain ruptures first. The GF, with lower elastic modulus and higher ultimate strain, then takes over and resists the load. As noted, if the stress at GF rupture is equal to or higher than that at CF rupture, which depends on a volume ratio of (GF/CF) (e.g., [2]), the pseudo-ductility can be obtained. Hybrid effects are also expected to be gained, such that it is possible to enhance (first) failure stress (or strain) beyond that predicted from the rule of mixtures, given Equation (7) below:

$$\boldsymbol{E_{HF} = E_{CF}\left(\frac{V_{CF}}{V_{HF}}\right) + E_{GF}\left(\frac{V_{GF}}{V_{HF}}\right)} \quad (7)$$

where E_{HF} is the weighted mean elastic modulus of a carbon-glass hybrid composite; E_{CF} and E_{GF} are the elastic moduli of CF and GF, respectively; V_{CF} and V_{GF} are the CF and GF volumes, respectively; and V_{HF} is the combined CF and GF volume or the volume of the hybrid composites.

Manders and Bader [2] reported that the increase in strain at CF rupture in sandwich laminated hybrids would be about 50% of that of single CF, and Aveston and Sillwood [19] also experimentally confirmed that the strain at CF rupture of hybrid carbon-glass-epoxy composites could be increased up to about 0.01. Furthermore, Miwa and Horiba [13] suggested the empirical rule of “hybrid” mixtures as:

$$\boldsymbol{f_{u\_C\_HF} = f_{u\_CF}\left(\frac{V_{CF}}{V_{HF}}\right) + f_{u\_GF}\left(\frac{V_{GF}}{V_{HF}}\right)} \quad (8)$$

where $f_{u\_C\_HF}$ is the mean stress of a carbon-glass hybrid composite at CF rupture and f_{u_CF} and f_{u_GF} are the ultimate stresses of CF and GF ruptures, respectively.

However, researchers (e.g., [2], [13]) did not reach any definite conclusion on the ultimate stress of hybrid carbon-glass composites at GF rupture. Pan and Postle [21] reported that due to the cross-coupling effects between the different fibers, a positive hybrid effect would be expected at the first fiber rupture, whereas a negative effect would be expected at the second fiber rupture; however, this appears to be the case only for the first fiber embedded in the matrix or a postulate without examination of an optimal ratio of two different fibers. It is not appropriate to apply the shear lag model [23] to the case of interest, since the hybrid sheet may have a substantially different degree of interfacial shear stress as in the case of a short-fiber embedded in the matrix. The increased or decreased strain (or stress) at GF rupture of the hybrid composites, particularly hybrid FRP sheets that are common in civil engineering applications, have not been well studied. A continuous FRP sheet consisting of fiber rovings may have a moderate level of frictional coupling between GF and CF rovings and behave very differently than the micro-composites with a high level of frictional coupling.

The current study consists of in-depth re-assessment of two hybrid material test programs conducted by collaborators, e.g. [24] and [25], who generously provided test data, identification of hybrid effects in the carbon-glass FRP sheets, and development of design models for stress-strain relationships with and without consideration of the hybrid effects. It is specifically noted that the author of this report conducted a detailed analysis of all raw data that were provided by Song et al. [25] and re-examined the results from the raw data thoroughly and meticulously to gain a better understanding of the behavior of the hybrid FRP sheets. This report includes the documentation of this research process and findings.

7. MATERIAL TEST PROGRAMS

Two independent material test programs on uniaxial hybrid fiber-reinforced polymer (FRP) sheets and each corresponding fiber used for the fabrication of the hybrid sheets are presented in this chapter. Note that although ACI 440.2R-08, Section 4.3.1 recommends using mean minus three times standard deviations for the ultimate stress and strain from at least 20 samples, the number for the tested sample was less than 20 for all three test programs.

7.1 FIRST TEST PROGRAM

Choi et al. [24] tested rovings of high-strength carbon fibers (CF) and E-glass fibers (GF) in tension, hybrid carbon-glass FRP sheets in tension, and epoxy adhesives in bending (J type as shown in Figure 11). Both bare and impregnated rovings were tested (Figures 12(a) and 12(b)), and digital data of forces and displacements at ultimate indicated by a Universal Test Machine (U.T.M; Lloyd Instruments, LR5K) with a 500 N (112 lbs) capacity were manually recorded. The cross-sectional areas of CF and GF rovings were 0.886 and 0.444 mm^2 (0.0014 and 0.0007 in^2), respectively. This is based on each material's Specific Gravity (ρ_{CF} = 1.8; ρ_{GF} = 2.54), and the measured weight and length. The impregnated roving tests were carried out in accordance with ASTM D3039-08. The test specimens had a total length of 400 mm (15.75 in.) and an effective length between yarn grips of 260 mm (10.25 in.). The tensile loading speed was 10 mm/min (0.4 in./min).

Figure 11 Four-Point Loading Tests of J and K Type Epoxy Resin Blocks (Choi et al. [24]; Song et al. [25]) (a) Bending testing of J type epoxy resin block (b) Bending testing of K type epoxy resin block

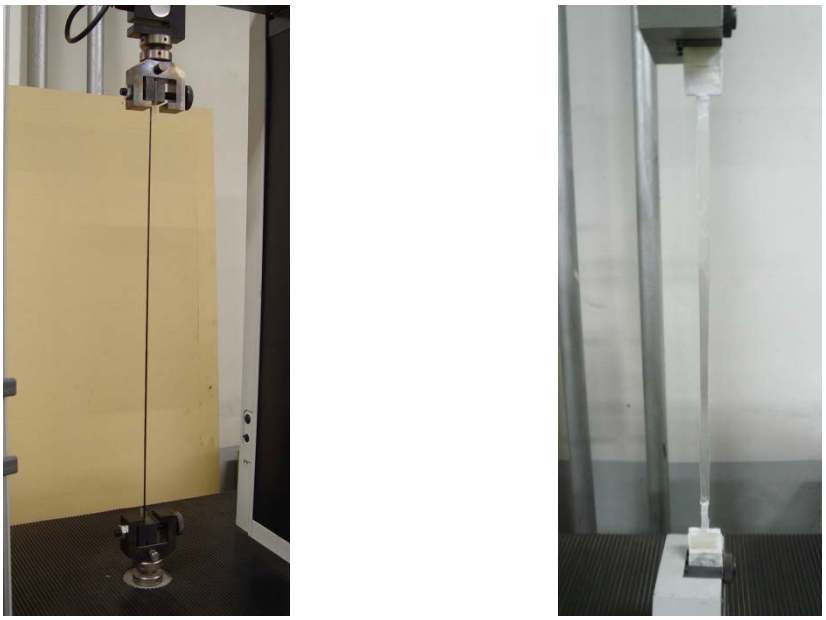

Figure 12 Tensile Tests of Non-Impregnated and Impregnated Fiber Rovings (Choi et al. [24]) (a) Tensile testing of bare CF roving (b) Tensile testing of impregnated GF roving

For the bar roving tests, a pair of thin, flat plastic films were laminated in the grips. For the impregnated roving tests, two different types of grips (Types A and B) were developed. The Type A grip tabs were applied using an epoxy adhesive. According to ASTM D3039-08, no industry consensus on the grip at the end of the fiber coupon is available. Thus, although grip failures were not observed from any of the methods used in the test program [24], an alternative method of gripping was developed, specifically, 90° sandwich laminates using the same fiber rovings (Type B grip). Table 4 summarizes the average of the results from rovings categorized as non-impregnated, impregnated-Type A grip and impregnated-Type B grip. As shown, there are no substantial discrepancies between the methods and within a method (standard deviations were relatively small), indicating that all of the test methods yield essentially consistent results.

Table 4 Provided Properties of CF and GF Filaments

	Carbon filament		Glass filament
σ_{u_CF}	4,900	σ_{u_GF}	2,900
ε_{u_CF}	0.0213	ε_{u_GF}	0.0401
E_{CF}	230	E_{GF}	72.4

Filament properties are provided by the manufacturer.
CF = Carbon fiber roving; GF = Glass fiber roving.
N = Non-impregnated rovings; A = Impregnated-Type A grip; B = Impregnated-Type B grip.
σ_{u_CF} Measured ultimate stress of CF roving [MPa].
ε_{u_CF} Measured ultimate strain of CF roving.
E_{CF} Measured elastic modulus of CF roving [GPa].
σ_{u_GF} Measured ultimate stress of GF roving [MPa].
ε_{u_GF} Measured ultimate strain of GF roving.
E_{GF} Measured elastic modulus of GF roving [GPa].
Conversion: 1 MPa = 0.145 ksi; 1 GPa = 145 ksi.

Table 5 Measured Results for the Uniaxial Tensile Tests of CF Rovings for CF-N series Conducted by Choi et al. [24]

	CF-N-1	CF-N-2	CF-N-3	CF-N-4	CF-N-5	CF-N-6	CF-N-7	Average
σ_{u_CF}	1,248	1,529	1,273	1,241	1,069	1,406	1,208	1,283
ε_{u_CF}	0.011	0.0123	0.0117	0.0114	0.01	0.0125	0.0105	0.0113
E_{CF}	114	125	109	109	107	113	115	113

Table 6 Measured Results for the Uniaxial Tensile Tests of CF Rovings for CF-A and CF-B series Conducted by Choi et al. [24]

	CF-A-1	CF-A-2	CF-A-3	CF-B-1	CF-B-2	CF-B-3	CF-B-4	CF-B-5	CF-B-6	Average
σ_{u_CF}	1,734	1,680	1,382	1,628	1,544	1,354	1,515	1,533	1,624	1,553

Table 7 Measured Results for the Uniaxial Tensile Tests of GF Rovings for GF-N series Conducted by Choi et al. [24]

	GF-N-1	GF-N-2	GF-N-3	GF-N-4	GF-N-5	GF-N-6	GF-N-7	GF-N-8	GF-N-9	GF-N-10	Average
σ_{u_GF}	708	883	757	776	901	769	801	794	785	742	792
ε_{u_GF}	0.0167	0.0185	0.0177	0.0167	0.0209	0.0191	0.0174	0.0166	0.0154	0.0169	0.0176
E_{GF}	42.3	47.8	42.9	46.4	43.2	40.3	46.0	47.8	51.1	43.9	45.1

Table 8 Measured Results for the Uniaxial Tensile Tests of GF Rovings for GF-A and GF-B series Conducted by Choi et al. [24]

	GF-A-1	GF-A-2	GF-A-3	GF-A-4	GF-A-5	GF-B-1	GF-B-2	GF-B-3	GF-B-4	GF-B-5	Average
σ_{u_GF}	580	584	869	571	661	1052	951	890	799	681	764

Carbon-glass hybrid FRP sheets were fabricated with a (GF/CF) volumetric ratio of (8.8/1) (see Figure 13), and tested in tension in accordance with CSA S806-02. Table 5 indicates the averaged values for three samples of the hybrid FRP sheets. Each sample has a cross-sectional area of about 17.5 mm^2 (0.027 in^2), with a 48K-CF roving of 1.8 mm^2 (0.0028 in^2) and eighteen 2,200tex-GF rovings of 15.6 mm^2 (0.024 in^2). Both strain gauges and LVDTs embedded in the U.T.M. (Instron) with a capacity of 1,200 kN (270 kips) were used to digitally monitor stains or displacement. In this study, the LVDT data were more reliable than the strain gauge data.

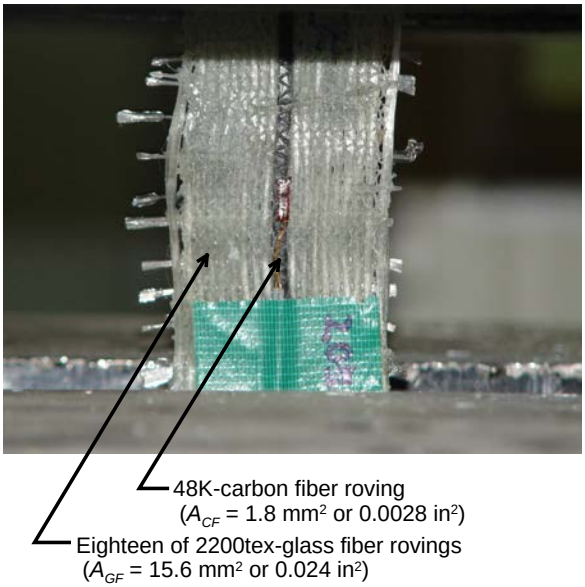

Figure 13 Tensile Testing of Hybrid Carbon-Glass FRP Sheet (Choi et al. [24])

In order to identify mechanical properties of epoxy adhesives, flexural tests were conducted instead of direct tensile tests. This is because, first, the flexural tests are much more convenient, and second, a tensile strain is generally smaller than the actual strain of the adhesive bonded to concrete (ASTM D638). In this study, epoxy solid blocks (J type) with dimensions of 25 x 25 x 240 mm (1 x 1 x 9.5 in.) were tested in flexure under four-point loading. The resulting average values of ultimate stress and strain and modulus of elasticity at rupture for three specimens are 42.8 MPa (6.2 ksi), 0.0197 and 2.19 GPa (317.6 ksi), respectively, which are similar to the typical values reported by ACI 503R-93. The ultimate strain of the product was relatively low. It would be useful to have an ultimate strain of about 0.04 to ensure that fiber ruptures prior to epoxy failure.

Table 9 Measured and Predicted Results for the Uniaxial Tensile Tests of Hybrid FRP Sheets with (GF/CF = 8.8/1) Conducted by Choi et al. [24]

Specimen	Meas. E_{HF} [GPa]	Meas. $\varepsilon_{u\_C\_HF}$	Meas. $\sigma_{u\_C\_HF}$ [MPa]	E_{HF}^{*} [GPa]	$\varepsilon_{u\_C\_HF}^{*}$	$\sigma_{u\_C\_HF}^{*}$ [MPa]	$\sigma_{u\_C\_HF}^{**}$ [MPa]	Meas. E_{GF}' [GPa]	Meas. $\varepsilon_{u\_G\_HF}$	Meas. $\sigma_{u\_G\_HF}$ [MPa]	$\sigma_{u\_G\_HF}^{*}$ [MPa]
(1)	(2)	(3)	(4)	(5)	(6)	(7)	(8)	(9)	(10)	(11)	(12)
Hybrid-1	59.2	0.0153	864.5	52	0.011	583.9	841.8	59	0.0218	1,040	711
Hybrid-2	67.1	0.0144	864.5	52	0.011	583.9	841.8	51.2	0.0181	928	711
Hybrid-3	68.5	0.0152	876.3	52	0.011	583.9	841.8	54	0.0228	1,277	711
Average	64.9	0.0150	868.4	52	0.011	583.9	841.8	54.7	0.0209	1,082	711

Meas. = Measured.
* = based on the rule of mixtures.
** = based on the rule of hybrid mixtures (Miwa and Horiba [13]).
E_{HF} Elastic modulus of hybrid FRP sheet.
$\sigma_{u\_C\_HF}$ Stress at CF rupture of hybrid FRP sheet.
$\varepsilon_{u\_C\_HF}$ Strain at CF rupture of hybrid FRP sheet.
E_{GF}' Average stress increase of hybrid FRP sheet divided by strain increase after CF rupture.
$\sigma_{u\_G\_HF}$ Stress at GF rupture of hybrid FRP sheet.
$\varepsilon_{u\_G\_HF}$ Strain at GF rupture of hybrid FRP sheet.
Conversion: 1 MPa = 0.145 ksi; 1 GPa = 145 ksi.

7.2 SECOND TEST PROGRAM

Song et al. [25] conducted tensile tests of conventional carbon and glass FRP sheets and hybrid carbon-glass FRP sheets with a variety of (GF/CF) ratios ranging from (1/1) to (10/1). Each sheet had a total length of about 250 mm (10 in.) (Figure 14). High-strength carbon fiber (CF) and E-glass fiber (GF) rovings were used along with two different types of epoxy resins (J type and K type) to fabricate a total of 99 impregnated hybrid sheet coupons. The J type epoxy is commonly used in practice, and the K type epoxy has a higher ductility. Tensile tests of the epoxy resins turned out to be infeasible due to the grip problem; thus, four-point loading tests were conducted on 25 x 25 x 240 mm (1 x 1 x 9.5 in.) molded epoxy blocks as shown in Figure 11. The ultimate strains for the J and K types were measured to be 0.02 and 0.029, respectively.

Using Specific Gravity (ρ_{CF} = 1.8 and ρ_{GF} = 2.54) and measured weights and lengths, the cross-sectional areas of CF and GF rovings were calculated to be 0.45 and 0.455 mm^2 (0.0007 and 0.000705 in^2), respectively. Controlling the number of each fiber roving (12K-CF roving and 1,200tex-GF roving), hybrid FRP sheets with 12 different (GF/CF) ratios were made (Table 6), including carbon FRP and glass FRP sheets. However, all the data from the glass FRP sheets were misplaced. Each sheet was impregnated with epoxy resin in a mold, where Overhead Projector (OHP) films were used to make the sample detachable from the mold. The width of the sample ranged from 11.9 to 16.5 mm (0.47 to 0.65 in.), and the strip thickness was 1.5 mm (0.06 in.) (Figure 14). An epoxy-to-fiber ratio of 1.5 was used.

Tension forces were digitally recorded from the Universal Test Machine (U.T.M), tensile strains from the strain gauges mounted on the impregnated FRP sheet and total elongations from the LVDTs. The tensile loading speed was 1 mm/min (0.04 in./min).

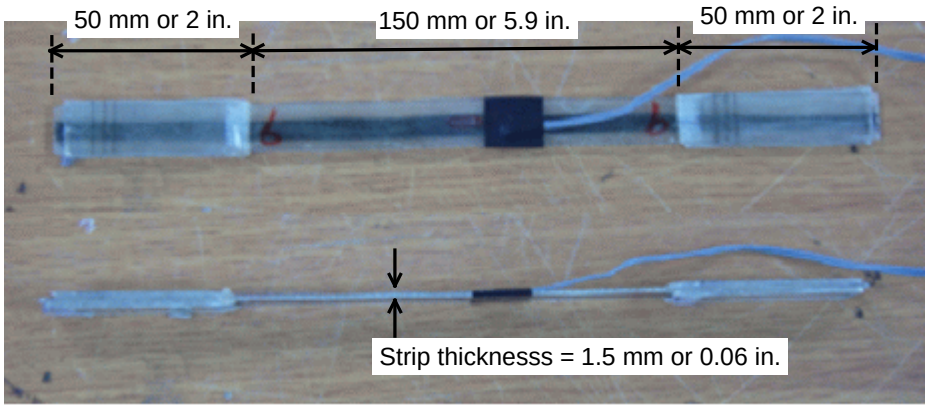

Figure 14 Impregnated Hybrid FRP Sheet Samples (Song et al. [25])

Table 10 Measured and Predicted Results of CFRP series for the Uniaxial Tensile Tests Conducted by Song et al. [25]

Specimen	Meas. E_{HF} [GPa]	Meas. $\varepsilon_{u\_C\_HF}$	Meas. $\sigma_{u\_C\_HF}$ [MPa]	E_{HF}^{*} [GPa]	$\varepsilon_{u\_C\_HF}^{*}$	$\sigma_{u\_C\_HF}^{*}$ [MPa]	$\sigma_{u\_C\_HF}^{**}$ [MPa]
(1)	(2)	(3)	(4)	(5)	(6)	(7)	(8)
CFRP-a	273.8	0.01	2,425	202	0.0129	2,656	3,474
CFRP-b	196	0.0125	2,450	202	0.0129	2,656	3,474
CFRP-c	189.7	0.0146	2,597	202	0.0129	2,656	3,474
CFRP-d	238.4	0.0105	2,496	202	0.0129	2,656	3,474
CFRP-e	194	0.0145	2,660	202	0.0129	2,656	3,474
CFRP-D-a	121.3	0.0108	2,404	202	0.0129	2,656	3,474
CFRP-D-b	233.7	0.0153	3,555	202	0.0129	2,656	3,474
CFRP-D-c	172.9	0.0154	2,662	202	0.0129	2,656	3,474
Average	202.4	0.013	2,656	202	0.0129	2,656	3,474

HFRP = Hybrid FRP sheet
D = Ductile K type epoxy.
1 → (GF/CF = 1/1); 2 → (GF/CF = 2/1); 3 → (GF/CF = 3/1); 4 → (GF/CF = 4/1); 5 → (GF/CF = 5.1/1);
6 → (GF/CF = 6.1/1); 7 → (GF/CF = 7.1/1); 8 → (GF/CF = 8.1/1); 9 → (GF/CF = 9.1/1); 10 → (GF/CF = 10.1/1).
* = based on the rule of mixtures.
** = based on the rule of hybrid mixtures (Miwa and Horiba [13]).
E_{HF} Elastic modulus of hybrid FRP sheet.
$\sigma_{u\_C\_HF}$ Stress at CF rupture of hybrid FRP sheet.
$\varepsilon_{u\_C\_HF}$ Strain at CF rupture of hybrid FRP sheet.
Conversion: 1 MPa = 0.145 ksi; 1 GPa = 145 ksi.

Table 11 Measured and Predicted Results of HFRP-1 series for the Uniaxial Tensile Tests Conducted by Song et al. [25]

Specimen	Meas. E_{HF} [GPa]	Meas. $\varepsilon_{u\_C\_HF}$	Meas. $\sigma_{u\_C\_HF}$ [MPa]	E_{HF}^{*} [GPa]	$\varepsilon_{u\_C\_HF}^{*}$	$\sigma_{u\_C\_HF}^{*}$ [MPa]	$\sigma_{u\_C\_HF}^{**}$ [MPa]	Meas. $E_{GF}^{'}$ [GPa]	Meas. $\varepsilon_{u\_G\_HF}$	Meas. $\sigma_{u\_G\_HF}$ [MPa]	$\sigma_{u\_G\_HF}^{*}$ [MPa]
HFRP-1-a	130.9	0.0157	2,057	134.7	0.0129	1,738	1,920				592
HFRP-1-b	164.9	0.0125	1,815	134.7	0.0129	1,738	1,920				592
HFRP-1-c	145.3	0.0152	2,202	134.7	0.0129	1,738	1,920	244.3	0.0173	4,473	592
HFRP-1-d	148	0.0179	2,644	134.7	0.0129	1,738	1,920				592
HFRP-1-e	156.5	0.0167	2,384	134.7	0.0129	1,738	1,920				592
HFRP-1-f	136.9	0.0142	1,945	134.7	0.0129	1,738	1,920				592
HFRP-1-g	130.9	0.0157	2,057	134.7	0.0129	1,738	1,920				592
HFRP-D1-a	150.5	0.0135	2,027	134.7	0.0129	1,738	1,920	208.9	0.0151	4,234	592
HFRP-D1-b	144.6	0.0133	1,873	134.7	0.0129	1,738	1,920	238.7	0.016	4,030	592
HFRP-D1-c	150.7	0.0134	2,077	134.7	0.0129	1,738	1,920				592
Average	146	0.0148	2,108	134.7	0.0129	1,738	1,920	230.6	0.0161	4,246	592

$E_{GF}^{'}$ Average increase in stress of hybrid FRP sheet after CF rupture divided by increase in strain.

$\sigma_{u\_G\_HF}$ Stress at GF rupture of hybrid FRP sheet.

$\varepsilon_{u\_G\_HF}$ Strain at GF rupture of hybrid FRP sheet.

Table 12 Measured and Predicted Results of HFRP-2 series for the Uniaxial Tensile Tests Conducted by Song et al. [25]

Specimen	Meas. E_{HF} [GPa]	Meas. $\varepsilon_{u\_C\_HF}$	Meas. $\sigma_{u\_C\_HF}$ [MPa]	E_{HF}^{*} [GPa]	$\varepsilon_{u\_C\_HF}^{*}$	$\sigma_{u\_C\_HF}^{*}$ [MPa]	$\sigma_{u\_C\_HF}^{**}$ [MPa]	Meas. $E_{GF}^{'}$ [GPa]	Meas. $\varepsilon_{u\_G\_HF}$	Meas. $\sigma_{u\_G\_HF}$ [MPa]	$\sigma_{u\_G\_HF}^{*}$ [MPa]
HFRP-2-a	259.8	0.0053	1,477	112.2	0.0129	1,447	1,675				790
HFRP-2-b	99.4	0.0156	1,578	112.2	0.0129	1,447	1,675	143.8	0.0186	2,014	790
HFRP-2-c	100.8	0.0135	1,357	112.2	0.0129	1,447	1,675	99.1	0.017	2,097	790
HFRP-2-d	100.9	0.0132	1,328	112.2	0.0129	1,447	1,675				790
HFRP-2-e	92.8	0.0154	1,427	112.2	0.0129	1,447	1,675	126.8	0.0161	1,589	790
HFRP-D2-a	126.7	0.0163	2,066	112.2	0.0129	1,447	1,675				790
HFRP-D2-b	121.3	0.0187	2,267	112.2	0.0129	1,447	1,675				790
HFRP-D2-c	106.5	0.018	1,756	112.2	0.0129	1,447	1,675				790
Average	126	0.0145	1,657	112.2	0.0129	1,447	1,675	123.2	0.0172	1,900	790

Table 13 Measured and Predicted Results of HFRP-3 series for the Uniaxial Tensile Tests Conducted by Song et al. [25]

Specimen	Meas. E_{HF} [GPa]	Meas. $\varepsilon_{u\_C\_HF}$	Meas. $\sigma_{u\_C\_HF}$ [MPa]	E_{HF}^{*} [GPa]	$\varepsilon_{u\_C\_HF}^{*}$	$\sigma_{u\_C\_HF}^{*}$ [MPa]	$\sigma_{u\_C\_HF}^{**}$ [MPa]	Meas. $E_{GF}^{'}$ [GPa]	Meas. $\varepsilon_{u\_G\_HF}$	Meas. $\sigma_{u\_G\_HF}$ [MPa]	$\sigma_{u\_G\_HF}^{*}$ [MPa]
HFRP-3-a	106.3	0.0191	2,039	101	0.0129	1,303	1,552				888
HFRP-3-b	89.1	0.0095	847	101	0.0129	1,303	1,552				888
HFRP-3-c	114.7	0.0135	1,553	101	0.0129	1,303	1,552				888
HFRP-3-d	117.5	0.013	1,527	101	0.0129	1,303	1,552	65.5			888
HFRP-3-e	111.8	0.0168	1,883	101	0.0129	1,303	1,552	111.8	0.0195	2,447	888
HFRP-3-f	91.6	0.0166	1,488	101	0.0129	1,303	1,552				888
HFRP-3-g	97.4	0.0124	1,203	101	0.0129	1,303	1,552				888
HFRP-D3-a	109.4	0.0171	1,875	101	0.0129	1,303	1,552				888
HFRP-D3-b	92.9	0.0164	1,590	101	0.0129	1,303	1,552				888
HFRP-D3-c	104.1	0.0184	1,914	101	0.0129	1,303	1,552				888
Average	103.5	0.0153	1,592	101	0.0129	1,303	1,552	88.7	0.0195	2,447	888

Table 14 Measured and Predicted Results of HFRP-4 series for the Uniaxial Tensile Tests Conducted by Song et al. [25]

Specimen	Meas. E_{HF} [GPa]	Meas. $\varepsilon_{u\_C\_HF}$	Meas. $\sigma_{u\_C\_HF}$ [MPa]	E_{HF}^{*} [GPa]	$\varepsilon_{u\_C\_HF}^{*}$	$\sigma_{u\_C\_HF}^{*}$ [MPa]	$\sigma_{u\_C\_HF}^{**}$ [MPa]	$\sigma_{u\_G\_HF}^{*}$ [MPa]
HFRP-4-a	107.5	0.0178	1,968	94.2	0.0129	1,215	1,479	948
HFRP-4-b	93.6	0.0185	1,729	94.2	0.0129	1,215	1,479	948
HFRP-4-c	88.3	0.021	1,854	94.2	0.0129	1,215	1,479	948
HFRP-4-d	101.6	0.0191	1,939	94.2	0.0129	1,215	1,479	948
HFRP-4-e	108.7	0.016	1,725	94.2	0.0129	1,215	1,479	948
HFRP-4-f	87.3	0.0193	1,684	94.2	0.0129	1,215	1,479	948
HFRP-4-g	96.9	0.0183	1,694	94.2	0.0129	1,215	1,479	948
HFRP-D4-a	98.7	0.0178	1,757	94.2	0.0129	1,215	1,479	948
HFRP-D4-b	104.5	0.0185	1,936	94.2	0.0129	1,215	1,479	948
HFRP-D4-c	103.6	0.0172	1,889	94.2	0.0129	1,215	1,479	948
Average	99.1	0.0184	1,818	94.2	0.0129	1,215	1,479	948

Table 15 Measured and Predicted Results of HFRP-5 series for the Uniaxial Tensile Tests Conducted by Song et al. [25]

Specimen	Meas. E_{HF} [GPa]	Meas. $\varepsilon_{u\_C\_HF}$	Meas. $\sigma_{u\_C\_HF}$ [MPa]	E_{HF}^{*} [GPa]	$\varepsilon_{u\_C\_HF}^{*}$	$\sigma_{u\_C\_HF}^{*}$ [MPa]	$\sigma_{u\_C\_HF}^{**}$ [MPa]	$\sigma_{u\_G\_HF}^{*}$ [MPa]
HFRP-5-a	77.9	0.0161	1,253	89.4	0.0129	1,153	1,426	990
HFRP-5-b	79.1	0.0197	1,556	89.4	0.0129	1,153	1,426	990
HFRP-5-c	31.9	0.0174	554	89.4	0.0129	1,153	1,426	990
HFRP-5-d	78.2	0.0178	1,362	89.4	0.0129	1,153	1,426	990
HFRP-5-e	80.3	0.0201	1,618	89.4	0.0129	1,153	1,426	990
HFRP-D5-a	69.8	0.0192	1,834	89.4	0.0129	1,153	1,426	990
HFRP-D5-b	97.2	0.018	1,753	89.4	0.0129	1,153	1,426	990
HFRP-D5-c	99	0.0185	1,834	89.4	0.0129	1,153	1,426	990
Average	76.7	0.0184	1,471	89.4	0.0129	1,153	1,426	990

Table 16 Measured and Predicted Results of HFRP-6 series for the Uniaxial Tensile Tests Conducted by Song et al. [25]

Specimen	Meas. E_{HF} [GPa]	Meas. $\varepsilon_{u\_C\_HF}$	Meas. $\sigma_{u\_C\_HF}$ [MPa]	E_{HF}^{*} [GPa]	$\varepsilon_{u\_C\_HF}^{*}$	$\sigma_{u\_C\_HF}^{*}$ [MPa]	$\sigma_{u\_C\_HF}^{**}$ [MPa]	Meas. $E_{GF}^{'}$ [GPa]	Meas. $\varepsilon_{u\_G\_HF}$	Meas. $\sigma_{u\_G\_HF}$ [MPa]	$\sigma_{u\_G\_HF}^{*}$ [MPa]
HFRP-6-a	74.4	0.0185	1,375	86.3	0.0129	1,113	1,392	71.2			1,018
HFRP-6-b	80.9	0.0175	1,417	86.3	0.0129	1,113	1,392				1,018
HFRP-6-c	80.9	0.0177	1,430	86.3	0.0129	1,113	1,392				1,018
HFRP-6-d	80.6	0.018	1,450	86.3	0.0129	1,113	1,392	84.1	0.0193	1,726	1,018
HFRP-6-e	78.5	0.0199	1,559	86.3	0.0129	1,113	1,392				1,018
HFRP-6-f	81.2	0.0193	1,565	86.3	0.0129	1,113	1,392				1,018
HFRP-D6-a	82.3	0.0178	1,465	86.3	0.0129	1,113	1,392	53.6	0.0233	1,511	1,018
HFRP-D6-b	92.6	0.0207	1,783	86.3	0.0129	1,113	1,392				1,018
HFRP-D6-c	93.8	0.0188	1,767	86.3	0.0129	1,113	1,392				1,018
Average	82.8	0.0187	1,535	86.3	0.0129	1,113	1,392	69.6	0.0213	1,619	1,018

Table 17 Measured and Predicted Results of HFRP-7 series for the Uniaxial Tensile Tests Conducted by Song et al. [25]

Specimen	Meas. E_{HF} [GPa]	Meas. $\varepsilon_{u\_C\_HF}$	Meas. $\sigma_{u\_C\_HF}$ [MPa]	E_{HF}^{*} [GPa]	$\varepsilon_{u\_C\_HF}^{*}$	$\sigma_{u\_C\_HF}^{*}$ [MPa]	$\sigma_{u\_C\_HF}^{**}$ [MPa]	Meas. $E_{GF}^{'}$ [GPa]	Meas. $\varepsilon_{u\_G\_HF}$	Meas. $\sigma_{u\_G\_HF}$ [MPa]	$\sigma_{u\_G\_HF}^{*}$ [MPa]
HFRP-7-a	68.2	0.0193	1,313	83.9	0.0129	1,082	1,366				1,038
HFRP-7-b	73.6	0.0173	1,269	83.9	0.0129	1,082	1,366				1,038
HFRP-7-c	61.9	0.0166	1,027	83.9	0.0129	1,082	1,366				1,038
HFRP-7-d	78.6	0.0158	1,248	83.9	0.0129	1,082	1,366				1,038
HFRP-7-e	66.8	0.0178	1,192	83.9	0.0129	1,082	1,366				1,038
HFRP-7-f	68	0.021	1,604	83.9	0.0129	1,082	1,366				1,038
HFRP-7-g	81.6	0.0176	1,464	83.9	0.0129	1,082	1,366	62.3	0.02	1,486	1,038
HFRP-D7-a	87.3	0.0193	1,682	83.9	0.0129	1,082	1,366	118.3	0.0229	1,918	1,038
HFRP-D7-b	91.6	0.0203	1,863	83.9	0.0129	1,082	1,366				1,038
HFRP-D7-c	79.7	0.0205	1,645	83.9	0.0129	1,082	1,366				1,038
Average	75.7	0.0186	1,431	83.9	0.0129	1,082	1,366	90.3	0.0215	1,702	1,038

Table 18 Measured and Predicted Results of HFRP-8 series for the Uniaxial Tensile Tests Conducted by Song et al. [25]

Specimen	Meas. E_{HF} [GPa]	Meas. $\varepsilon_{u\_C\_HF}$	Meas. $\sigma_{u\_C\_HF}$ [MPa]	E_{HF}^{*} [GPa]	$\varepsilon_{u\_C\_HF}^{*}$	$\sigma_{u\_C\_HF}^{*}$ [MPa]	$\sigma_{u\_C\_HF}^{**}$ [MPa]	Meas. $E_{GF}^{'}$ [GPa]	Meas. $\varepsilon_{u\_G\_HF}$	Meas. $\sigma_{u\_G\_HF}$ [MPa]	$\sigma_{u\_G\_HF}^{*}$ [MPa]
HFRP-8-a	71.4	0.018	1,286	82.1	0.0129	1,059	1,346				1,054
HFRP-8-b	73.1	0.0211	1,543	82.1	0.0129	1,059	1,346				1,054
HFRP-8-c	71.3	0.0173	1,236	82.1	0.0129	1,059	1,346				1,054
HFRP-8-d	74.9	0.02	1,454	82.1	0.0129	1,059	1,346	40.1			1,054
HFRP-8-e	73.7	0.0184	1,356	82.1	0.0129	1,059	1,346	58.2	0.0233	1,359	1,054
HFRP-8-f	88	0.0206	1,811	82.1	0.0129	1,059	1,346	56	0.0251	1,772	1,054
HFRP-8-g	79.8	0.0221	1,766	82.1	0.0129	1,059	1,346	49			1,054
HFRP-D8-a	85.4	0.0179	1,529	82.1	0.0129	1,059	1,346				1,054
HFRP-D8-b	82.2	0.0184	1,514	82.1	0.0129	1,059	1,346				1,054
HFRP-D8-c	89.8	0.0141	1,263	82.1	0.0129	1,059	1,346				1,054
Average	79	0.0188	1,476	82.1	0.0129	1,059	1,346	50.8	0.0242	1,566	1,054

Table 19 Measured and Predicted Results of HFRP-9 series for the Uniaxial Tensile Tests Conducted by Song et al. [25]

Specimen	Meas. E_{HF} [GPa]	Meas. $\varepsilon_{u\_C\_HF}$	Meas. $\sigma_{u\_C\_HF}$ [MPa]	E_{HF}^{*} [GPa]	$\varepsilon_{u\_C\_HF}^{*}$	$\sigma_{u\_C\_HF}^{*}$ [MPa]	$\sigma_{u\_C\_HF}^{**}$ [MPa]	Meas. $E_{GF}^{'}$ [GPa]	Meas. $\varepsilon_{u\_G\_HF}$	Meas. $\sigma_{u\_G\_HF}$ [MPa]	$\sigma_{u\_G\_HF}^{*}$ [MPa]
HFRP-9-a	84.2	0.0211	1,777	80.6	0.0129	1,040	1,330	92.8	0.0245	1,766	1,067
HFRP-9-b	87.2	0.0211	1,837	80.6	0.0129	1,040	1,330	107.2	0.0235	1,833	1,067
HFRP-9-c	89.1	0.0203	1,807	80.6	0.0129	1,040	1,330	79.5	0.0251	1,841	1,067
HFRP-9-d	101.8	0.0193	1,697	80.6	0.0129	1,040	1,330				1,067
HFRP-9-e	99.4	0.0171	1,717	80.6	0.0129	1,040	1,330	53.8	0.0233	1,865	1,067
HFRP-9-f	94.5	0.0192	1,986	80.6	0.0129	1,040	1,330	67.2			1,067
HFRP-9-g	78.5	0.0201	1,580	80.6	0.0129	1,040	1,330				1,067
HFRP-D9-a	84.4	0.0187	1,645	80.6	0.0129	1,040	1,330	36.2	0.0192	1,715	1,067
HFRP-D9-b	92.3	0.0162	1,149	80.6	0.0129	1,040	1,330	20.6	0.0222	1,560	1,067
HFRP-D9-c	82.9	0.0223	1,548	80.6	0.0129	1,040	1,330				1,067
Average	89.4	0.0195	1,674	80.6	0.0129	1,040	1,330	65.3	0.023	1,763	1,067

Table 20 Measured and Predicted Results of HFRP-10 series for the Uniaxial Tensile Tests Conducted by Song et al. [25]

Specimen	Meas. E_{HF} [GPa]	Meas. $\varepsilon_{u\_C\_HF}$	Meas. $\sigma_{u\_C\_HF}$ [MPa]	E_{HF}^{*} [GPa]	$\varepsilon_{u\_C\_HF}^{*}$	$\sigma_{u\_C\_HF}^{*}$ [MPa]	$\sigma_{u\_C\_HF}^{**}$ [MPa]	Meas. $E_{GF}^{'}$ [GPa]	Meas. $\varepsilon_{u\_G\_HF}$	Meas. $\sigma_{u\_G\_HF}$ [MPa]	$\sigma_{u\_G\_HF}^{*}$ [MPa]
HFRP-10-a	73.8	0.0209	1,544	79.4	0.0129	1,024	1,,317				1,078
HFRP-10-b	74.7	0.021	1,568	79.4	0.0129	1,024	1,317	100.8			1,078
HFRP-10-c	70.2	0.0205	1,439	79.4	0.0129	1,024	1,317				1,078
HFRP-D10-a	86.5	0.0187	1,621	79.4	0.0129	1,024	1,317				1,078
HFRP-D10-b	85	0.0171	1,396	79.4	0.0129	1,024	1,317	66.7	0.0205	1,494	1,078
HFRP-D10-c	88.3	0.0143	1,305	79.4	0.0129	1,024	1,317				1,078
Average	79.8	0.0188	1,479	79.4	0.0129	1,024	1,317	83.8	0.0205	1,494	1,078

This Page is Intentionally Blank

8. THE RULE OF MIXTURES

Chou and Kelly [12] and Manders and Bader [2] proposed a tensile stress model for hybrid carbon-glass FRP composites, as shown in Figure 15, based on the rule of mixtures. Points A and D denote the ultimate tensile stresses when GF and CF, respectively, are used alone (i.e., GF = 100%; CF = 100%). Also, the lines A-E and B-D represent the mean stresses in hybrid FRP when GF and CF fail, respectively. The CF with lower ε_{u_CF} than ε_{u_GF} (or higher $E_{\_CF}$ than $E_{\_GF}$) always fails prior to GF. To the right of Point C, after the first failure of CF, the hybrid FRP has a very low residual mean stress that is only provided by GF (i.e., brittle failure). To the left of Point C, even after the first failure of CF, the hybrid FRP with a relatively large amount of GF can sustain more loads without a drop in strength until the GF rupture. As such, pseudo-ductility can be achieved with this combination.

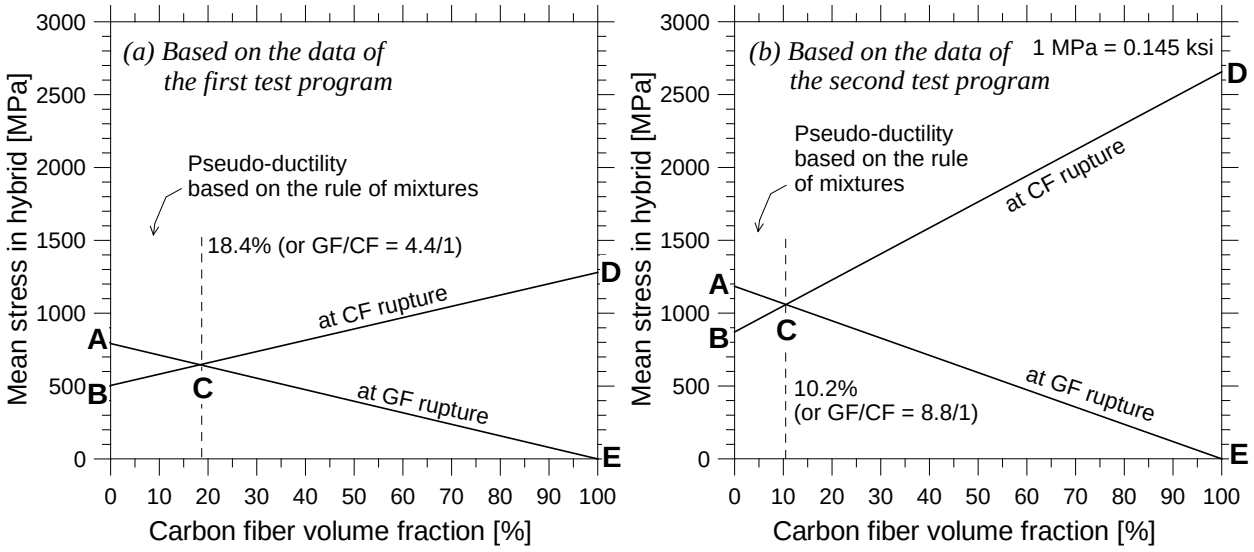

Figure 15 The Rule of Mixtures

Points A and D are taken as f_{u_CF} and f_{u_GF}, respectively, which can be obtained from the roving or sheet tests. The mean stress at Point B is calculated as ε_{u_CF} times E_{GF}, where ε_{u_CF} is the measured average ultimate strain of the CF roving/sheet and E_{GF} is the measured elastic modulus of the GF roving/sheet. Using the rule of mixtures and the material properties, the x-axis value at Point C is determined (e.g., (4.4/1) for Choi et al. [24]). The ratios of (4.4/1) and (8.8/1) are equivalent to the carbon volume fractions of 18.4% and 10.2%, respectively. The y-axis value can be obtained from a cross point of two straight lines drawn in Figure 15(a) or 15(b).

To determine the stress (f_{HF}) in hybrid FRP for a given tensile strain (ε_{HF}), the rule of mixtures is applied as follows:

If $\varepsilon_{HF} \leq \varepsilon_{u\_CF}$ $$\boldsymbol{f_{HF} = \left[E_{CF}\left(\frac{A_{CF}}{A_{HF}}\right) + E_{GF}\left(\frac{A_{GF}}{A_{HF}}\right)\right]\varepsilon_{HF}} \text{ or } \boldsymbol{f_{HF} = E_{HF}\varepsilon_{HF}} \quad (9)$$

If $\varepsilon_{u\_CF} < \varepsilon_{HF} \leq \varepsilon_{u\_GF} \times (A_{GF}/A_{HF})$ $$\boldsymbol{f_{HF} = E_{GF}\varepsilon_{HF}} \quad (10)$$

where ε_{HF} and f_{HF} are the strain and stress in hybrid FRP (variables), respectively; ε_{u_CF} and ε_{u_GF} are the ultimate strains of CF and GF, respectively; E_{CF} and E_{GF} are the elastic moduli of CF and GF, respectively; A_{CF} and A_{GF} are the cross-sectional areas of CF and GF in a hybrid sheet coupon, and A_{HF} is $(A_{CF} + A_{GF})$.

Equations (9) and (10) are consistent with Figure 15. For example, when the fiber roving properties reported by Choi et al. [24] are considered and the carbon volume fraction is 18.4%, the stress of f_{HF} is calculated to be $[(0.184E_{CF} + 0.816E_{GF}) \times \varepsilon_{HF}]$ at CF rupture, which is represented by Point C in Figure 15(a). Once CF rupture occurs Equation (10) is applicable and the stress at GF rupture is assumed to be the same as $[\varepsilon_{u\_GF}E_{GF} \times (A_{GF}/A_{HF})]$. This failure is represented by the line A-E in Figure 15.

9. ASSESSMENT OF TEST RESULTS

Based on the information relevant to the mechanical properties of materials obtained in the test programs, an attempt was made to identify two different hybrid effects: 1) improved mechanical properties until the first peak, and 2) those after the first peak. Assessment of the data was carefully undertaken in this section.

9.1 FIRST TEST PROGRAM

First, the roving tensile properties were obtained (Table 4). Using each fiber's Specific Gravity (ρ_{CF} = 1.8; ρ_{GF} = 2.54) and measured weight per unit length, the cross-sectional area was determined to be 0.444 and 0.866 mm^2 (6.9 x 10^{-4} and 1.34 x 10^{-3} in^2) for the tested CF and GF rovings, respectively. The weight of the fiber roving was measured using a digital scale with an accuracy of +/–0.01 g (or 2.2 x 10^{-5} lbs).

Results from the tensile tests are presented in Table 4. In the remainder of the paper, the mean stress and strain (f_u and ε_u) from the non-impregnated (bare) coupon tests were used (though both results are similar). This is because epoxy resins are typically applied on only one side of the FRP sheet. The roving results for ultimate stress (f_u), ultimate strain (ε_u) and elastic modulus (E) in tension are substantially lower than the filament properties provided by the manufacturer (Table 4). This is due to the fragmentation process that generates unequal tension of filaments within a roving and failure strain variation between the filaments. Such phenomena are also seen from the behavior of conventional FRP sheets externally bonded to the concrete surface.

As indicated in Table 5 (compare Columns (4) and (7), and (11) and (12)), both stresses at CF and GF ruptures in hybrid FRP sheets with a (GF/CF) ratio of (8.8/1) were higher than the theoretical values, respectively. These positive hybrid effects can be seen as a result of the synergistic strengthening of both fibers. In particular, the ultimate stress and strain were increased by about 38% and 25%, respectively, compared with those of the GF roving. The corresponding stiffness after the first peak (CF rupture) was 54.5 MPa (7,903 ksi), about 20% larger than the elastic modulus (45 MPa or 6,525 ksi) of the

GF roving. Tensile stress-strain relations of 2 samples of the hybrid FRP sheets are plotted in Figure 16, where the LVDT data were used to determine strains, in comparison with that of steel. Again, it is noted that the stress was calculated as the measured load divided by the cross-sectional areas of A_{HF} until the first peak (CF rupture) and A_{GF} after CF rupture.

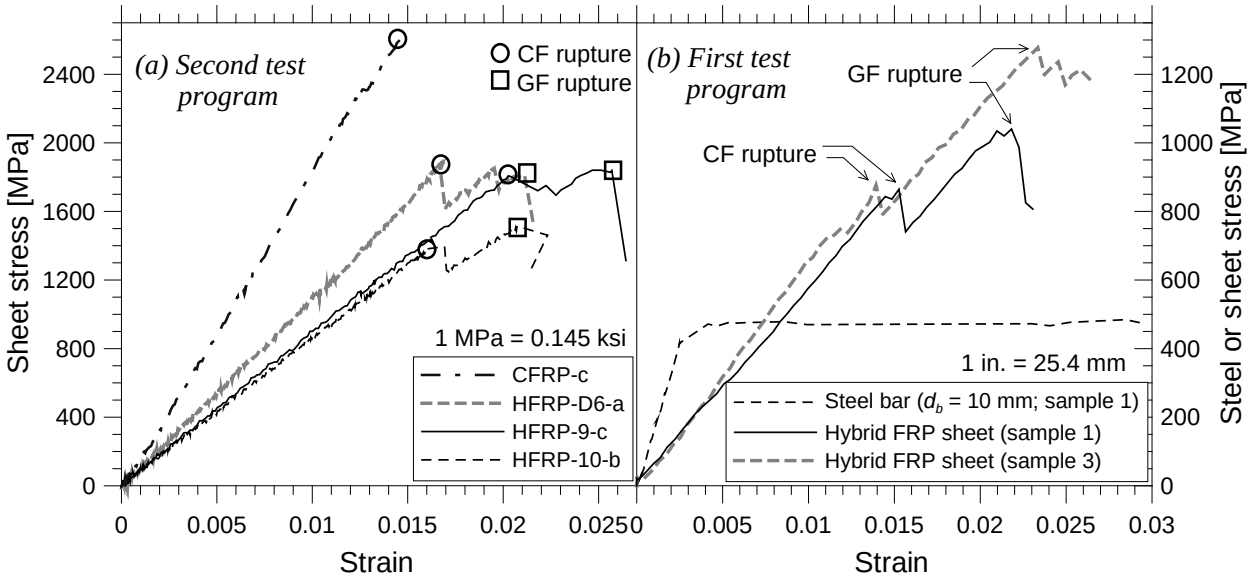

Figure 16 Measured Stress-Strain Curves of Selected Carbon FRP and Hybrid FRP Sheets and Conventional Steel

9.2 SECOND TEST PROGRAM

In this study, the roving properties of each fiber were not obtained; rather, the impregnated carbon FRP and glass FRP sheets were tested in tension to obtain each fiber's properties. Unfortunately, the results of the impregnated glass FRP sheets were misplaced; thus, the ultimate strain (ε_{u_GF} = 0.0176) from the roving tests of Choi et al. [24] is adopted for further analysis, as the fibers used for both programs were manufactured by the same vendor. For the elastic modulus of GF, the average stiffness

of the hybrid sheets after CF rupture can be generally taken into account assuming that the Young's modulus (E_{GF} = 67.3 GPa; 9,760 ksi) is almost the same as that of GF. Finally, the ultimate stress (f_{u_GF} = 1,185 MPa; 172 ksi) is taken as the product of 0.0176 and 67.3 GPa (9,760 ksi).

Figure 16 shows selected results of the impregnated carbon FRP and hybrid FRP sheets. The stress was taken to be the load divided by the cross-sectional area of the whole fibers until CF rupture and by the area of the glass fibers only after CF rupture. The cross-sectional area of the sheet was determined based on the number of each fiber roving and its cross-sectional area estimated using the roving weight and Specific Gravity (ρ_{CF} = 1.8; ρ_{GF} = 2.54), where the weight was measured using a micro-digital scale with an accuracy of +/–1 x 10^{-5} g (or 2.2 x 10^{-8} lbs). This does not include the area of the epoxy. In addition, it appears that the type of epoxy resins did not affect the tensile behavior of the sheets much. There was no clear evidence of different performance between the sheets impregnated using the J type and K type epoxy resins.

The ultimate stresses (average f_{u_CF} = 2,656 MPa or 372 ksi) and elastic moduli (average E_{CF} = 202 MPa or 29,360 ksi) of the impregnated carbon FRP sheets are lower than those (f_{u_CF} = 4,900 MPa or 710.5 ksi; E_{CF} = 230 GPa or 33,350 ksi) of a carbon filament that the manufacturer reported. The differences are much less compared with those between the filament and rovings. The average ultimate strain (ε_{u_CF}) of the CF sheets is 0.013, which is smaller than all but three of 91 ultimate strains (average $\varepsilon_{u\_C\_HF}$ = 0.018) of the hybrid sheet coupons at CF rupture. This is evidently due to the hybrid effect. For the hybrid FRP sheets, the ratio of (GF/CF) also affected the overall behavior. As the (GF/CF) ratio increased, both the strains at CF and GF ruptures generally increased (Table 6). In the following chapter, more detailed investigations are conducted in connection with the theoretical models.

This Page is Intentionally Blank

10. COMPARISON WITH THE RULE OF MIXTURES

Experimental results corresponding to line B-D in Figure 15 are obtained using the measured strains of hybrid FRP coupons at CF rupture and the measured loads, summarized in Column (4) of Tables 2 and 3, and depicted in Figures 17(a) and 17(b). The significantly increased stresses relative to line B-D are noted. The average strain ($\varepsilon_{u\_C\_HF}$) at CF rupture is also about 35% higher than ε_{u_CF}. For (GF/CF) ratios higher than (4.4/1), an increase of about 45% occurred, whereas for (GF/CF) ratios lower than (4.4/1), the increase was about 22%. In general, the value of $\varepsilon_{u\_C\_HF}$ increases as the (GF/CF) ratio increases. This indicates that a constant increase in failure strain, when the hybrid effect is expected, may not be valid (e.g., 50% or 0.01 strain increase). The difference between the measured stresses of $f_{u\_C\_HF}$ and the predicted stresses of $f_{u\_C\_HF}$ based on Equation (8) is only about 10% (see Columns (4) and (8) of Tables 2 and 3), indicating that the rule of "hybrid" mixtures suggested by Miwa and Horiba [13] works better than the rule of mixtures for fiber composites, which underestimates the experimental values by about 35%.

Based on these results, the positive hybrid effect is evident for hybrid FRP sheets that are usually used for repair and retrofit of the concrete structures, and these hybrid effects include the stress and strain of the hybrid FRP sheet at CF rupture (but not Young's modulus). The Young's modulus of the hybrid FRP sheet until CF rupture is almost the same as that of the carbon FRP sheet (1% difference on average).

Similarly, experimental results corresponding to the line A-E in Figure 15 are examined. The average stress ($f_{u\_G\_HF}$ = 1,094 MPa or 158.6 ksi) at GF rupture was monitored from 3 specimens of Choi et al. [24] with the (GF/CF) ratio of (8.8/1). This is about 40% higher than the corresponding point [f_{u_GF} x (A_{GF}/A_{HF})] = 771 MPa or 103.2 ksi) in Figure 17(c) (see Column (12) of Table 5). The average ultimate strain ($\varepsilon_{u\_G\_HF}$ = 0.022) of the

hybrid FRP is also higher by 40% relative to the product (= 0.0158) of ε_{u_GF} and (A_{GF}/A_{HF}). This is clearly inconsistent with the rule of mixtures. The average increase in stress after CF rupture divided by the average increase in strain (54.7 GPa or 7,076 ksi) is also somewhat higher than the elastic modulus (E_{GF} = 45 GPa or 6,525 ksi) of the GF roving (by about 20%).

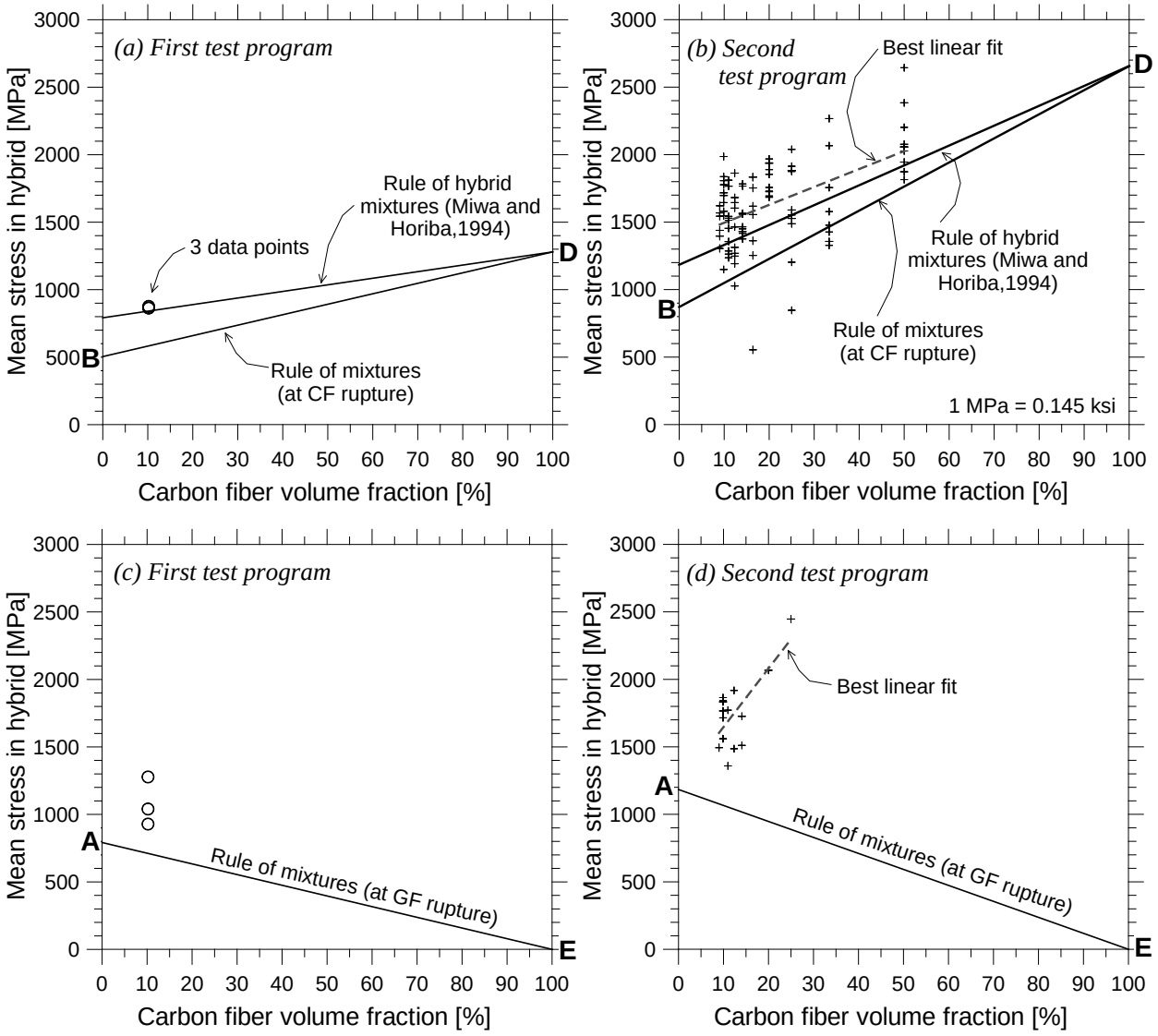

Figure 17 Identification of Hybrid Effects

Unlike the test program of Choi et al. [24], the GF rupture was not captured well for many specimens of the second test program (Song et al. [25]) because of the strain gauge or epoxy failure prior to GF rupture, and the disruption of testing once the strain gauge or epoxy failed. Therefore, direct comparisons between $f_{u\_G\_HF}$ and (f_{u_GF} x [GF/(GF+CF)]) or between ε_{u_GF} and ($\varepsilon_{u\_G\_HF}$ x [GF/(GF+CF)]) are not possible due to the absence of the GF properties. The averages of the 14 measured values of $f_{u\_G\_HF}$ and $\varepsilon_{u\_G\_HF}$ are 1,759 MPa (255 ksi) and 0.022, respectively, which are generally higher than the roving test results of Choi et al. [24]. Interestingly, there is a tendency of increasing failure stress ($f_{u\_G\_HF}$) with decreasing (GF/CF) ratio or increasing carbon volume fraction (Figure 17). This means that both the initial stiffness and pseudo-ductility can be obtained even with lower (GF/CF) ratios (see Figures 16(a), 18 and 19). While the trend opposite to the rule of mixtures is noteworthy, the data appear not to indicate different ultimate strains depending on the (GF/CF) ratio (versus ultimate stresses). There is a need for further experimental investigation for the ultimate stress and strain in relation with the (GF/CF) ratio.

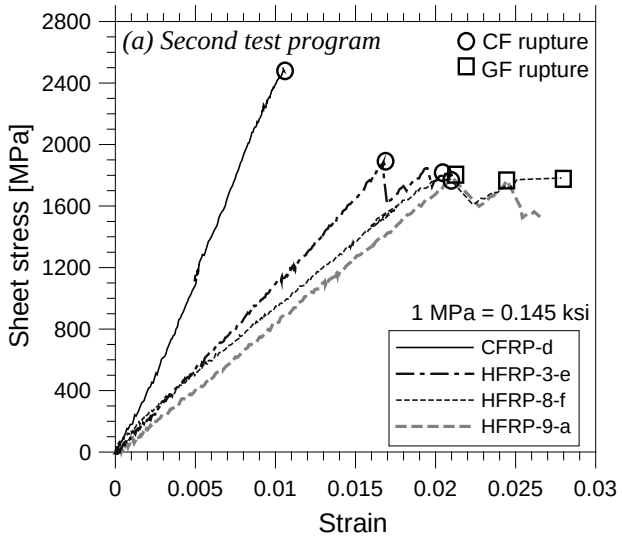

Figure 18 Pseudo-Ductility of Hybrid FRP Sheets Noted From Measured Stress-Strain Curves

Based on the two independent programs investigated, it can be concluded that the hybrid effects are positive in terms of the ultimate stress and strain at GF rupture for all (GF/CF) ratios. Note that these positive effects are contrary to the prediction made by

Pan and Postle [21] for micro-fibers embedded in the matrix. This seems to be related to the degree of coupling between two different fibers. The use of hybrid FRP sheets consisting of CF and GF rovings has been proven to be a very effective means to promote synergistic hybrid effects. In a similar manner, the hybrid effect of uniaxial hybrid FRP sheets that are made of 3 different fiber rovings could be investigated.

Figure 16(a) shows the stress-strain relationship for the 2 coupons tested by Choi et al. [24], where pseudo-ductility was observed. This is consistent with the rule of mixtures which suggests the recovery of the stress after CF rupture when a point representing the (GF/CF) ratio is located to the left of Point C in Figure 15. On the other hand, the data reported from the second test program exhibit a high degree of ductility after CF rupture even for low (GF/CF) ratios (Figures 16(a) and 18). Because the data are quite limited, additional tests would be helpful to evaluate the stress recovery after CF rupture.

11. PROPOSED STRESS-STRAIN RELATIONSHIP FOR HYBRID FRP SHEETS

When the moment and shear capacities of concrete members strengthened with hybrid FRP sheets are determined, a stress-strain or force-strain relationship of the hybrid FRP sheets would be needed. The stress-strain relationship of Equations (9) and (10), which is based on the rule of mixtures, does not account for the identified positive hybrid effects. In this study, based on the review on the test results, the following stress-strain relationship for hybrid carbon-glass hybrid FRP sheets is proposed.

If $\varepsilon_{HF} \leq \varepsilon_{u\_C\_HF}$

$$\boldsymbol{f_{HF} = E_{HF}\varepsilon_{HF} = \left[E_{CF}\left(\frac{A_{CF}}{A_{HF}}\right) + E_{GF}\left(\frac{A_{GF}}{A_{HF}}\right)\right]\varepsilon_{HF}} \quad (11)$$

If $\varepsilon_{u\_C\_HF} < \varepsilon_{HF} \leq \varepsilon_{u\_G\_HF}$

$$\boldsymbol{f_{HF} = E_{GF}\varepsilon_{HF}} \quad (12)$$

where $\varepsilon_{u\_C\_HF}$ is taken as ($f_{u\_C\_HF}/E_{HF}$); $f_{u\_C\_HF}$ can be estimated using Eq (2); and $\varepsilon_{u\_G\_HF}$ is the strain of hybrid FRP sheets at GF rupture, suggested to be approximately 0.022 when a (GF/CF) ratio is larger than (4/1), respectively. The suggested values are based on the re-assessed data from the two test programs. It is noted that the elastic moduli in the proposed stress-strain relationship do not reflect the positive hybrid effect since the increased properties are minor. Also, note that after CF rupture, the stress of f_{HF} should be paired with A_{GF} (not A_{HF}) to determine the force, assuming that CF no longer resists any tension.

The analytical stress-strain relationships with and without consideration of hybrid effects are depicted in Figure 19 for a variety of (GF/CF) ratios. The former is expressed in the form of Equations (11) and (12), while the latter is expressed in the form of Equations. (9) and (10). It is noted that $\varepsilon_{u\_C\_HF}$ is a function of the (GF/CF) ratio, whereas a fixed value of $\varepsilon_{u\_G\_HF}$ of 0.022 is proposed. Also, strains of ε_{u_CF} and ε_{u_GF} are suggested to be 0.013 and 0.018, respectively, and elastic moduli of E_{CF} and E_{GF} to be 202 GPa (29,300 ksi) and 67 GPa (9,700 ksi). If the rule of mixtures is applied, pseudo-ductility can only be achieved when a (GF/CF) ratio is not less than (8.8/1) (Figure 19(a)). If the hybrid

effect is considered, which has been demonstrated in this study, pseudo-ductility is characterized in almost all (GF/CF) ratios (Figure 19(b)). Furthermore, a strain at CF rupture is even higher than that at the second fiber (GF) rupture without the consideration of the hybrid effect (Figures 19(c) and 19(d)). This is one of the greatest advantages that hybridized carbon and glass fibers can offer. Regarding the effect of the (GF/CF) ratio, the hybrid model shows better performance in terms of the stiffness for lower (GF/CF) ratios, and the same ductility for all (GF/CF) ratios, still substantially higher than that of CF or GF. Such behaviors are also seen in Figures 16(a) and 18. However, a high (GF/CF) ratio (e.g., 8.7/1) is recommended because the reduction of the cross-sectional area of the FRP sheet with a very low (GF/CF) is drastic and cost effectiveness is at its maximum when the highest (GF/CF) ratio is used.

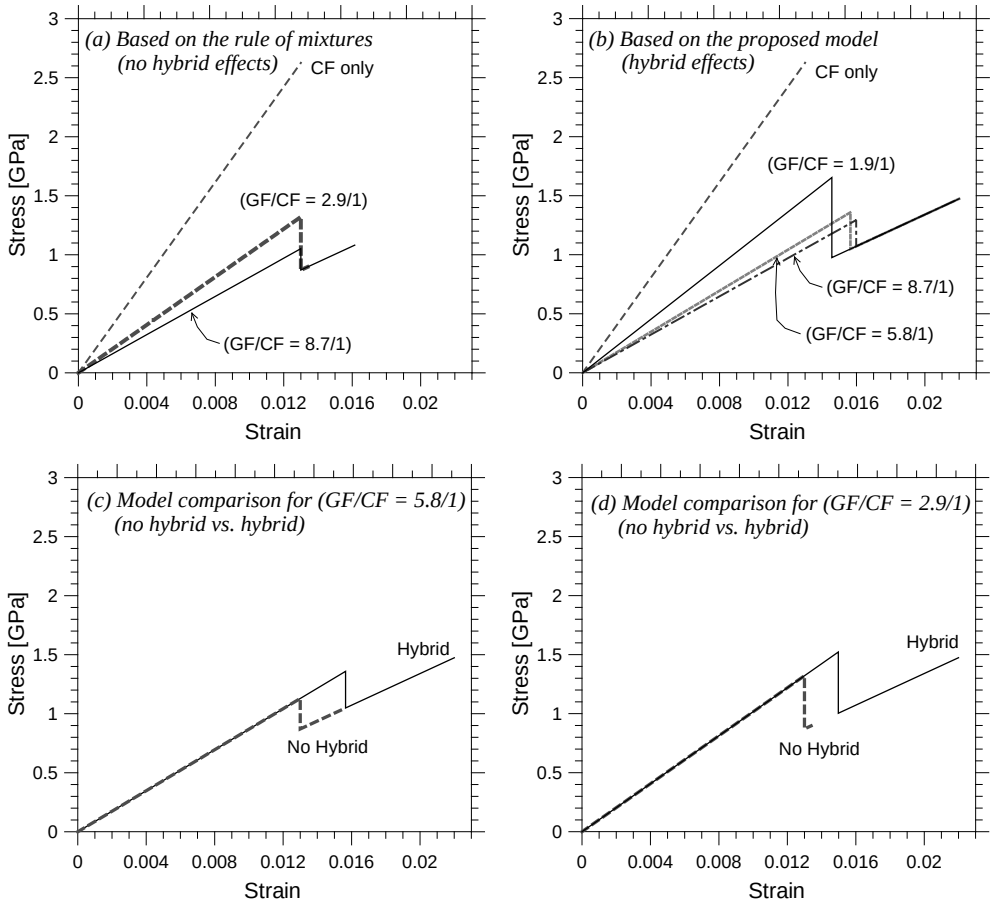

Figure 19 Models for Stress-Strain Relationship of Hybrid FRP Sheets with Various (GF/CF) Ratios

12. CONCLUSIONS OF PART II

The purposes of the use of uniaxial hybrid FRP sheets in the repair of existing concrete structures are to achieve pseudo-ductility and utilize their hybrid effects. In this study, the tensile test results from a total of 94 hybrid carbon-glass FRP sheets and 47 carbon and glass fiber rovings or sheets were evaluated and reviewed in depth. Based on this review, a number of conclusions are made as follows:

1. The three types of grips developed by Choi et al. [24] for the roving tests are effective. In particular, the grip with 90° sandwich laminates using the same fiber rovings appears to be very sound.

2. The two epoxy resins (J and K types) sustained strains up to about 0.02 and 0.03, respectively; however, an ultimate strain of about 0.04 is recommended to prevent epoxy failure prior to fiber rupture. Neither type of the epoxy resins affected the tensile behavior of the sheets much.

3. The elastic moduli of hybrid FRP sheets generally correspond to the rule of mixtures.

4. The strains at CF and GF ruptures of the hybrid sheets are about 0.018 and 0.022, respectively, on average, which are substantially higher than the ultimate strains of each CF and GF (0.013 and 0.018). A trend of increased strain at CF rupture for increased (GF/CF) ratio was observed, while there is no clear indication of different strains at GF rupture depending on the (GF/CF) ratio.

5. The stresses at CF rupture of the hybrid sheets are also significantly higher than those predicted based on the rule of mixtures, differing by about 40%, but are quite close to those predicted based on the rule of hybrid mixtures developed by Miwa and Horiba [13] (within about 10% difference). Also, the stresses at GF rupture are considerably higher than those predicted based on the rule of

mixtures, by about 80%. The discovery of these positive hybrid effects is a significant advance.

6. A general trend of increased stress at GF rupture for decreased (GF/CF) ratio was observed. This signals that both the initial stiffness and pseudo-ductility could be obtained even with a very low (GF/CF) ratio. However, given the limited data, additional research would be needed to verify this trend.

7. The identified hybrid effects are evident for all (GF/CF) ratios. When carbon and glass fibers are hybridized, an ultimate strain at the first fiber (carbon) rupture could be even higher than the ultimate strain of the second fiber (glass only).

8. The positive hybrid effects at both CF and GF ruptures might be shown only in the hybrid FRP sheets that are made of CF and GF rovings. If each fiber had been mixed in a roving, the positive hybrid effects might have not been found.

REFERENCES

[1] Phillips, L. N., “The Hybrid Effect-Does It Exist?,” *Composites*, 7, Jan. 1976, pp. 7-8.

[2] Manders, P. W. and Bader, M. G., “The Strength of Hybrid Glass/Carbon Fibre Composites: Part 1 – Failure Strain Enhancement and Failure Mode,” *Journal of Materials Science*, 16, 1981, pp. 2233-2245.

[3] Harris, H. G.; Somboonsong, W.; and Frank, K. K., “New Ductile Hybrid FRP Reinforcing Bar for Concrete Structures,” *ASCE Journal of Composites for Construction*, 2(4), 1998, pp. 28-36.

[4] Wu, G.; Wu, Z. S.; Lu, Z.; and Ando, Y. B., “Structural Performance of Concrete Confined with Hybrid FRP Composites,” *Journal of Reinforced Plastics and Composites*, 27(12), Aug. 2008, pp. 1323-1348.

[5] Grace, N. F.; Abel-Sayed, G.; and Ragheb, W. F., “Strengthening of Concrete Beams Using Innovative Ductile Fiber-Reinforced Polymer Fabric,” *ACI Structural Journal*, 99(5), Sept.-Oct. 2002, pp. 692-700.

[6] ACI Committee 440, “Guide for the Design and Construction of Externally Bonded FRP Systems for Strengthening Concrete Structures (ACI 440.2R-02),” ACI, Farmington Hills, Mich., 2002, 45 pp.

[7] ISIS Canada Design Manual No. 4, “Strengthening Reinforced Concrete Structures with Externally-Bonded Fibre Reinforced Polymers,” ISIS Canada Research Network, Sept. 2001, Winnipeg, Canada.

[8] ACI Committee 503, “Use of Epoxy Compounds with Concrete (ACI 503R-93; Reapproved 1998),” ACI, Farmington Hills, Mich., 1998, 28 pp.

[9] ASTM International, ASTM D638-08 Standard Test Method for Tensile Properties of Plastics, West Conshohocken, Penn: ASTM International, 2008, p. 16.

[10] ACI Committee 503, Guide for the Selection of Polymer Adhesives in Concrete (ACI 503.5R-92; Reapproved 2003), Farmington Hills, Mich: ACI, 2003, p. 16.

[11] ASTM International, “ASTM D3039/D3039M-08 Standard Test Method for Tensile Properties of Polymer Matrix Composite Materials,” ASTM International, West Conshohocken, Penn., 2008, 13 pp.

[12] Chou, T.-W. and Kelly, A., “Mechanical Properties of Composites,” *Annual Reviews of Material Science*, 10, 1980, pp. 229-259.

[13] Miwa, M. and Horiba, N., “Effects of Fibre Length on Tensile Strength of Carbon/Glass Fibre Hybrid Composites,” *Journal of Materials Science*, 29, 1994, pp. 973-997.

[14] CAN/CSA S806-02 (R2007), “Design and Construction of Building Components with Fibre-Reinforced Polymers,” CSA, Mississauga, Canada, 2007, pp. 206.

[15] ACI Committee 318, “Building Code Requirements for Structural Concrete (ACI 318-08) and Commentary (318R-08),” ACI, Farmington Hills, Mich., 2008, pp. 456.

[16] CSA-A23.3-94 (R2000), “Design of Concrete Structures,” CSA, Mississauga, Canada, 2000, pp. 199.

[17] Tomii, M., “Ductile and Strong Columns Composed of Steel Tube, Infilled Concrete and Longitudinal Bars,” *Proc. 3rd Int. Conf. on Steel-Concrete Composite Structures*, Fukuoda, Japan, 1991, pp. 39-66.

[18] Bunsell, A. R. and Harris, B., “Hybrid Carbon and Glass Fibre Composites,” *Composites*, 5, 1974, pp. 157-164.

[19] Aveston, J. and Sillwood, J. M., “Synergistic Fibre Strengthening in Hybrid Composites,” *Journal of Materials Science*, 11(10), 1976, pp. 1877-1883.

[20] Marom, G., Fischer, S., Tuler, F. R. and Wagner, H. D., “Hybrid Effects in Composites: Conditions for Positive or Negative Effects versus Rule of Mixtures,” *Journal of Materials Science*, 13, 1978, pp. 1419-1426.

[21] Pan, N. and Postle, R., “Tensile Strengths and the Hybrid Effects of Hybrid Fibre Composites: A Probabilistic Approach,” *Transitions of the Royal Society in London*, Series A., 354, 1996, pp. 1875-1897.

[22] Nanni, A., Henneke, M. J. and Okamoto, T., “Tensile Properties of Hybrid Rods for Concrete Reinforcement,” *Construction and Building Materials*, 8(1), 1994, p 27-34.

[23] Cox, H. L., “The Elasticity and Strength of Paper and Other Fibrous Materials,” *British Journal of Applied Physics*, 3, 1952, pp. 72-79.

[24] Choi, D.-U., Kang, T. H.-K., Ha, S.-S., Kim, K.-H. and Kim, W., “Flexural and Bond Behavior of Concrete Beams Strengthened with Hybrid Carbon-Glass Fiber-Reinforced Polymer Sheets," *ACI Structural Journal*, 108(1), Jan. 2011, pp. 90-98.

[25] Song, H., Min, C. and Lee, C., "Tensile Behavior of Hybrid Fiber," *Academic Conference Proceedings of Korean Society of Civil Engineers*, Gangwon-do, Korea, 2009, 4 pp. (in Korean)